European Journal of Medicinal Chemistry 143 (2018) 1474–1488

Contents lists available at ScienceDirect

European Journal of Medicinal Chemistry

journal homepage: http://www.elsevier.com/locate/ejmech

Research paper

Design, synthesis and biological evaluation of novel aryldiketo acids with enhanced antibacterial activity against multidrug resistant bacterial strains

Ilija N. Cvijetić [a, **], Tatjana Ž. Verbić [b], Pedro Ernesto de Resende [c], Paul Stapleton [c], Simon Gibbons [c], Ivan O. Juranić [d], Branko J. Drakulić [d, 1], Mire Zloh [e, *]

[a] Innovation Center of the Faculty of Chemistry, University of Belgrade, Studentski trg 16, Belgrade, Serbia
[b] Faculty of Chemistry, University of Belgrade, Studentski trg 16, Belgrade, Serbia
[c] UCL School of Pharmacy, University College London, London, UK
[d] Institute of Chemistry, Technology and Metallurgy, Department of Chemistry, University of Belgrade, Njegoševa 12, Belgrade, Serbia
[e] University of Hertfordshire, College Lane, Hatfield, AL10 9AB, UK

ARTICLE INFO

Article history:
Received 3 July 2017
Received in revised form
4 October 2017
Accepted 15 October 2017
Available online 11 November 2017

Keywords:
Aryl diketo acid
Antimicrobial activity
Multidrug resistance
Gram-positive
3D QSAR
Molecular docking
Dehydrosqualene synthase

ABSTRACT

Antimicrobial resistance (AMR) is a major health problem worldwide, because of ability of bacteria, fungi and viruses to evade known therapeutic agents used in treatment of infections. Aryldiketo acids (ADK) have shown antimicrobial activity against several resistant strains including Gram-positive *Staphylococcus aureus* bacteria. Our previous studies revealed that ADK analogues having bulky alkyl group in ortho position on a phenyl ring have up to ten times better activity than norfloxacin against the same strains. Rational modifications of analogues by introduction of hydrophobic substituents on the aromatic ring has led to more than tenfold increase in antibacterial activity against multidrug resistant Gram positive strains.

To elucidate a potential mechanism of action for this potentially novel class of antimicrobials, several bacterial enzymes were identified as putative targets according to literature data and pharmacophoric similarity searches for potent ADK analogues. Among the seven bacterial targets chosen, the strongest favorable binding interactions were observed between most active analogue and *S. aureus* dehydrosqualene synthase and DNA gyrase. Furthermore, the docking results in combination with literature data suggest that these novel molecules could also target several other bacterial enzymes, including prenyl-transferases and methionine aminopeptidase. These results and our statistically significant 3D QSAR model could be used to guide the further design of more potent derivatives as well as in virtual screening for novel antibacterial agents.

1. Introduction

Growing bacterial resistance toward commonly used antibiotics represents a major health problem for the community. After the discovery of penicillin, the boost in antibiotics discovery was between the 1950s and 1960s, but after 1985 the number of newly discovered antibiotics rapidly decreased [1]. Another problem arises from the fact that the majority of recently discovered antibiotics belong to already known classes of antibiotics. With the occurrence of *Staphylococcus aureus* strains resistant even to the drugs of last resort such as vancomycin [2] it is clear that we need antibiotics with an alternative mode of action.

Isoprenoid biosynthesis, catalyzed by enzymes prenyl transferases, is an interesting new target for antibacterial drug discovery. One of prenyl transferases, undecaprenyl diphosphate synthase (UPPS), is involved in early stages of bacterial cell wall biosynthesis and represents an excellent target for drug design since UPPS is not produced in humans [3]. Another interesting target is dehydrosqualene synthase (CrtM), an enzyme involved in the formation of *S. aureus* virulence factor staphyloxanthin. Inhibition of CrtM

* Corresponding author.
** Corresponding author.
E-mail addresses: ilija@chem.bg.ac.rs (I.N. Cvijetić), zloh@live.co.uk (M. Zloh).
[1] Authors regret to inform that Branko Drakulić has passed away since completion of the research for this paper.

https://doi.org/10.1016/j.ejmech.2017.10.045
0223-5234/

makes bacteria more sensible to host-derived reactive oxygen species [4,5] and it is one of the potential targets for development of antimicrobial agents.

Diketo acids are known inhibitors of HIV-1 integrase (IN). Structural similarity between fluoroquinolone antibiotics and aryldiketo acids (ADK, Fig. 1) inspired initial research of ADKs as antibacterial agents, initially reported by our group [6] that revealed an antibacterial activity of ADK previously not reported for this class of compounds. It was discovered that bulky hydrophobic substituents on the aromatic ring of the ADK were responsible for the increase of their antibacterial activity.

IN active site contains Mg^{2+}/Asp motif and diketo acids IN inhibitors are able to sequestrate Mg^{2+} ion from the active site [7]. Since all prenyl transferases also possess Mg^{2+}/Asp motif (Fig. 2), it was hypothesized and confirmed that diketo acids having a large hydrophobic moiety inhibit UPPS and CrtM, and also have notable activity against many Gram-positive bacteria [8].

In this study, we report rational design, synthesis and antibacterial activity of novel ADK derivatives, designed using previously reported findings [6] against several MDR bacterial strains. Additional derivatives similar to ADK, without parts of diketo-acid moiety, were also synthesized and tested in order to confirm the importance of this part of the molecule for antibacterial activity. Along with this, structure-activity relationship (SAR) study highlighted the structural features important for the antibacterial activity of ADKs against MDR *S. aureus* strain. In this study, several physicochemical properties important for pharmacokinetics assessment (human serum albumin binding, acidity constants, and lipophilicity) are determined for the most potent ADK derivative.

2. Materials and methods

2.1. Synthesis and characterization

All chemicals for the synthesis of ADK were purchased from Fluka, Aldrich, or Merck, having >98% purity, and were used as received. For the thin-layer chromatography, silica gel pre-coated plates with fluorescent indicator (254 nm) were used.

Melting points were determined in open capillary tubes on Stuart SMP-10 apparatus and are uncorrected. ESI-MS analysis was performed in methanol on an Agilent Technologies 6210-1210 TOF-LC-ESI-MS instrument in positive or negative mode. IR spectra were recorded on a Thermo Nicolet 6700 FT-IR spectrometer equipped with ATR accessory. ^{1}H and ^{13}C NMR spectra were recorded in DMSO-d_6, $CDCl_3$ or CD_3OD at 298 K using a Varian Gemini 2000 200/50 MHz or Bruker Avance 500/125 MHz NMR instrument.

ADKs were synthesized through the *Claisen* condensation between substituted acetophenones and diethyl oxalate, as previously described (Fig. 3) [6,9].

Some substituted acetophenones, which were not commercially available, were synthesized through the *Friedel-Crafts* acylation of corresponding benzene.

For the synthesis of **17**–**20**, *para*-amino substituted acetophenones were synthesized according to the following procedure: in a high-pressure, bomb-type reactor, 5 mmol of 4-fluoroacetophenone, 20 mmol of corresponding cyclic secondary amine and 3 ml of acetone were added. After heating for 3 h at 180 °C, the reaction mixture was poured into water, and extracted with ethyl acetate or chloroform. Combined organic layers were dried over sodium sulphate, concentrated under vacuum, and purified by crystallization or column chromatography.

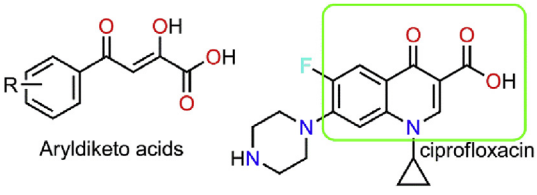

Fig. 1. Structural similarity of phenyl-substituted aryldiketo acids and ciprofloxacin.

Compounds **1a**-**3a** were synthesized through the *Friedel-Crafts* acylation of corresponding benzene with succinic anhydride. The identity and purity of compounds were confirmed using ^{1}H and ^{13}C NMR spectroscopy (Figs. S1–S25), IR spectroscopy, melting point determination, and LC-HR/ESI-MS. Synthesis and characterization of compounds **1**–**3**, **5**–**7** was described previously [10].

(*Z*)-2-hydroxy-4-oxo-4-(*o*-tolyl)but-2-enoic acid (2): $C_{11}H_{10}O_4$, M_r = 206.19, white powder, (1.25 g, 76%), mp = 106–108 °C, dcc (crystallized from EtOH); ESI-MS: Calculated for $C_{11}H_9O_4$ $[M-H]^-$ 205.0501, found 205.0509; IR (ν, cm^{-1}): 2991 *br* (COO–H), 1710 (C=O), 1635 (C=O), 1279 (C–O); ^{1}H NMR (200 MHz, DMSO-d_6) δ (ppm): 2.46 (s, 3 H), 4.48 (*s*, *br*, C$\underline{H}_2$ from diketo form), 6.71 (s, 1 H, C$\underline{H}$ of enol form), 7.35 (t, 1 H, overlapped with signal at 7.31), 7.31 (d, 1 H), 7.48 (t, J = 7.30 Hz, 1 H), 7.68 (*d*, J = 8,42 Hz, 1 H); ^{13}C NMR (50 MHz, DMSO-d_6) δ (ppm): 20.62, 51.78, 101.69, 126.32, 129.04, 131.83, 132.13, 135.86, 137.50, 163.35, 168.48, 194.81.

(*Z*)-2-hydroxy-4-oxo-4-(*m*-tolyl)but-2-enoic acid (3): $C_{11}H_{10}O_4$, M_r = 206.19, white powder (0.82 g, 73%), mp = 98–99 °C (crystallized from EtOH), ESI-MS: Calculated for $C_{11}H_9O_4$ $[M-H]^-$ 205.0501, found 205.0508; IR (ν, cm^{-1}): 3501 *br* (COO–H), 1683 (C=O), 1628 (C=O), 1257 (C–O); ^{1}H NMR (200 MHz, DMSO-d_6) δ (ppm): 2.36 (s, 3 H), 4.53 (*s*, *br*, C$\underline{H}_2$ from diketo form), 7.06 (s, 1 H, C$\underline{H}$ of enol form), 7.41 (t, J = 7.99 Hz, 1 H), 7.45 (*d*, J = 7,99 Hz, 1 H), 7.79 (d, J = 7.99 Hz, 1 H), 7.83 (s, 1 H); ^{13}C NMR (50 MHz, DMSO-d_6) δ (ppm): 20.84, 53.13, 97.95, 125.15, 128.30, 129.08, 134.70, 134.78, 138.72, 163.30, 170.30, 190.70.

(*Z*)-4-(4-butylphenyl)-2-hydroxy-4-oxobut-2-enoic acid (4): $C_{14}H_{16}O_4$, M_r = 248.27, white powder (4.82 g, 82%), mp = 145–147 °C; ESI-MS: Calculated for $C_{14}H_{17}O_4$ $[M+H]^+$ 249.1121, found 249.1113; IR (ν, cm^{-1}): 3007 *br*, 1714, 1628, 1272; ^{1}H NMR (200 MHz, $CDCl_3$) δ (ppm): 0.93 (t, J = 7.30 Hz, 3 H), 1.36 (*sx*, J = 7.30, 15.16 Hz, 2 H), 1,63 (*qn*, J = 7.86 Hz, 2 H), 2.69 (*t*, J = 7.86, 15.16 Hz, 2 H), 3.94 (*s*, *br*, C$\underline{H}_2$ from diketo form), 7.15 (s, 1 H, C$\underline{H}$ of enol form), 7.31 (d, J = 8.42 Hz, 2 H), 7.92 (d, J = 7.86 Hz, 2 H); ^{13}C NMR (50 MHz, $CDCl_3$) δ (ppm): 13.98, 22.42, 33.24, 35.93, 96.49, 128.29, 129.28, 131.36, 150.63, 163.65, 171.89, 188.82.

(*Z*)-4-(2,4-dimethylphenyl)-2-hydroxy-4-oxobut-2-enoic acid (5): $C_{12}H_{12}O_4$, M_r = 220.22, pale yellow powder (5.21 g, 78%), mp = 123–124 °C (crystallized from AcOEt/PhMe), ESI-MS: Calculated for $C_{12}H_{11}O_4$ $[M-H]^-$ 219.0657, found 219.0663; IR (ν, cm^{-1}): 2969 *br* (COO–H), 1710 (C=O), 1633 (C=O), 1271 (C–O); ^{1}H NMR (200 MHz, $CDCl_3$) δ (ppm): 2.38 (s, 3 H), 2.55 (s, 3 H), 6.96 (*s*, C$\underline{H}$ of enol form, 1 H), 7.11–7.15 (m, 2 H, overlapped *d* and *s* from *m*-H atoms), 7.60 (d, J = 8.40 Hz, 1 H); ^{13}C NMR (50 MHz, $CDCl_3$) δ (ppm): 21.44, 100.77, 126.86, 129.66, 131.75, 133.08, 139.16, 143.63, 164.70, 168.50, 194.17.

(*Z*)-2-hydroxy-4-oxo-4-(2,4,5-trimethylphenyl)but-2-enoic acid (6): $C_{13}H_{14}O_4$, M_r = 234.25, pale yellow powder (4.58 g, 68%), mp = 139–141 °C (crystallized from AcOEt/PhMe), ESI-MS: Calculated for $C_{13}H_{13}O_4$ $[M-H]^-$ 233.0819, found 233.0821; IR (ν, cm^{-1}): 2925 *br* (COO–H), 1709 (C=O), 1619 (C=O), 1275 (C–O); ^{1}H NMR (200 MHz, DMSO-d_6) δ (ppm): 2.24 (s, 6 H), 2.43 (s, 3 H), 4.47 (*s*, *br*, C$\underline{H}_2$ from diketo form), 6.80 (s, 1 H, C$\underline{H}$ of enol form), 7.10 (s, 1 H), 7.52 (s, 1 H); ^{13}C NMR (50 MHz, DMSO-d_6) δ (ppm): 18.65, 19.35, 20.52, 51.46, 101.23, 130.31, 132.81, 133.27, 134.29, 135.50, 141.66, 163.43, 167.80, 195.23.

(*Z*)-2-hydroxy-4-oxo-4-(2,3,5,6-tetramethylphenyl)but-2-enoic acid (7): $C_{14}H_{16}O_4$, Mr = 248.27, white powder (5.20 g, 78%),

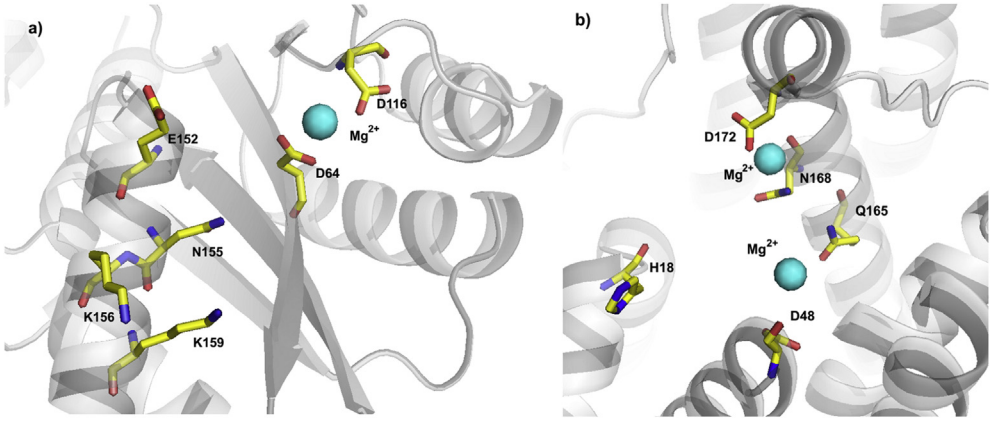

Fig. 2. Active sites of: a) HIV-1 integrase (PDB code 1K6Y); b) CrtM (PDB code 4F6V).

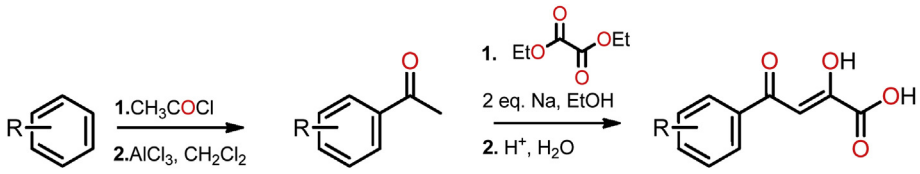

Fig. 3. Synthetic procedure for aryldiketo acids.

mp = 156–158 °C, dcc, (crystallized from AcOEt/PhMe), ESI-MS: Calculated for $C_{14}H_{15}O_4$ $[M-H]^-$ 247.0976, found 247.0976; IR (ν, cm^{-1}): 2962 *br* (COO–H), 1743 (C=O), 1599 (C=O), 1261 (C–O); ^1H NMR (200 MHz, DMSO-d_6) δ (ppm): 2.04 (s, 6 H), 2.17 (s, 6 H), 6.21 (s, 1 H, CH of enol form), 7.02 (s, 1 H); ^{13}C NMR (50 MHz, DMSO-d_6) δ (ppm): 15.98, 19.29, 103.77, 129.19, 132.00, 133.87, 138.70, 163.77, 169.17, 196.89.

(*Z*)-2-hydroxy-4-oxo-4-(5,6,7,8-tetrahydronaphthalen-2-yl) but-2-enoic acid (8): $C_{14}H_{14}O_4$, M_r = 246.26, white powder (0.84 g, 63%), mp = 173–175 °C (crystallized from AcOEt/PhMe), ESI-MS: Calculated for $C_{14}H_{15}O_4$ $[M+H]^+$ 247.0965, found 247.0963; IR (ν, cm^{-1}): 3382 *br*, 1642, 1591, 1421; ^1H NMR (200 MHz, $CDCl_3$) δ (ppm): 1.81 (m, 4 H), 2,82 (*m*. 4H), 7.12 (s, 1 H), 7.17 (d, J = 8.42 Hz, 1 H), 7.69 (m, 2 H, overlapped signals of two *o*-H atoms); ^{13}C NMR (50 MHz, $CDCl_3$) δ (ppm): 22.74, 22.88, 29.40, 29.86, 96.83, 125.15, 129.01, 129.92, 131.25, 138.17, 145.05, 164.18, 171.04, 189.54.

1-(4-ethyl-2,6-diisopropylphenyl)ethanone (5a): $C_{17}H_{26}O$, M_r = 246.39, white powder (3.12 g, 69%), mp = 79–80 °C (crystallized from AcOEt/PhMe); ESI-MS: Calculated for $C_{17}H_{27}O$ $[M+H]^+$ 247.2056, found 247,2063; ^1H NMR (200 MHz, $CDCl_3$) δ (ppm): 1.23–1.26 (*m*, overlapped doublets, 18 H), 2.50 (s, 3 H), 2.73 (*hp*, J = 6.74 Hz, 2 H), 2.89 (*hp*, J = 6.74 Hz, 1 H), 7.01 (s, 2 H); ^{13}C NMR (50 MHz, $CDCl_3$) δ (ppm): 24.07, 24.47, 31.09, 34.06, 34.42, 121.17, 138.50, 143.25, 149.54, 209.59.

(*Z*)-2-hydroxy-4-oxo-4-(2,4,6-triisopropylphenyl)but-2-enoic acid (9): $C_{19}H_{26}O_4$, M_r = 318.41, white powder (0.75 g, 56%), mp = 152–153 °C (crystallized from AcOEt/PhMe), ESI-MS: Calculated for $C_{19}H_{27}O_4$ $[M+H]^+$ 319.1904, found 319.1903; IR (ν, cm^{-1}): 3024 *br*, 1712, 1626, 1277; ^1H NMR (200 MHz, $CDCl_3$) δ (ppm): 1.25 (overlapped *d*, 18 H), 2.88 (*hp*, 3 H), 3.91 (*s*, *br*, CH_2 of diketo form), 6.56 (*s*), 6.65 (s, 1 H), 7.05 (two overlapped *s*, 2 H); ^{13}C NMR (50 MHz, $CDCl_3$) δ (ppm): 24.01, 24.49, 31.10, 31.19, 34.56, 53.36, 103.17, 104.69, 121.27, 121.36, 132.12, 133.61, 145.03, 145.36, 150.91, 151.28, 162.74, 163.30, 168.58, 171.82, 196.64, 199.45. Multiple tautomeric forms are observed in solution.

4-oxo-4-(2,4,6-triisopropylphenyl)butanoic acid (2a): $C_{19}H_{28}O_3$, M_r = 304.42, white powder, mp = 126–128 °C (crystallized from PhMe); ESI-MS: Calculated for $C_{19}H_{29}O_3$ $[M+H]^+$ 305.2111, found 305.2102; IR (ν, cm^{-1}): 2989 *br*, 1688, 1224; ^1H NMR (200 MHz, $CDCl_3$) δ (ppm): 1.23 (d, J = 4.6 Hz, 12 H), 1.27 (d, J = 4.7 Hz, 6 H), 2.71 (*hp*, overlapped, 2 H), 2.79 (*t*, J = 6.18, 12.92 Hz, 2 H), 2,90 (*hp*, overlapped, 1 H), 3.05 (*t*, J = 6.74, 12.92 Hz, 2 H), 7.02 (s, 2 H); ^{13}C NMR (50 MHz, $CDCl_3$) δ (ppm): 24.13, 24.48, 27.78, 30.98, 34.47, 40.89, 121.24, 137.20, 143.91, 149.89, 179.07, 208.79.

4-([1,1′-biphenyl]-4-yl)-4-oxobutanoic acid (3a): $C_{16}H_{14}O_3$, M_r = 254.28, white powder, mp = 157–159 °C (crystallized from PhMe); IR (ν, cm^{-1}): 3034 *br*, 1706, 1263; ^1H NMR (200 MHz, DMSO-d_6) δ (ppm): 2.60 (t, J = 6.18 Hz, 2 H), 3.28 (t, J = 6.18 Hz, 2 H), 7.46 (m, 1 H), 7.52 (d, J = 7.86 Hz, 2 H), 7.74 (d, J = 7.86 Hz, 2 H), 7.82 (d, J = 8.42 Hz, 2 H), 8.02 (d, J = 8.42 Hz, 2 H). ^{13}C NMR (50 MHz, DMSO-d_6) δ (ppm): 27.91, 33.16, 125.21, 126.98, 127.06, 128.66, 129.18, 135.31, 138.97, 144.61, 173.95, 198.13.

(*Z*)-2-hydroxy-4-(4-methoxy-2,5-dimethylphenyl)-4-oxobut-2-enoic acid (10): $C_{13}H_{14}O_5$, M_r = 250.25, pale yellow powder (2.39 g, 85%), mp = 167–169 °C, dcc (crystallized from AcOEt/PhMe), ESI-MS: Calculated for $C_{13}H_{13}O_5$ $[M-H]^-$ 249.0768, found 249.0766; IR (ν, cm^{-1}): 2948 *br*, 1713, 1621, 1277; ^1H NMR (200 MHz, DMSO-d_6) δ (ppm): 2.17 (s, 3 H), 2.53 (s, 3 H), 3.87 (s, 3 H), 4.46 (*s*, *br*, CH_2 of diketo form), 6.86 (s, 1 H, CH of enol form), 6.91 (s, 1 H), 7.63 (s, 1 H); ^{13}C NMR (50 MHz, DMSO-d_6) δ (ppm): 15.39, 21.79, 51.19, 55.68, 100.99, 113.91, 123.57, 126.88, 132.13, 139.58, 160.71, 163.55, 166.51, 194.83.

(*Z*)-2-hydroxy-4-(4-hydroxy-3,5-dimethylphenyl)-4-oxobut-2-enoic acid (11): $C_{12}H_{12}O_5$, M_r = 236.22, white powder (0.89 g, 70%), mp = 191–193 °C (crystallized from EtOH), ESI-MS: Calculated for $C_{12}H_{13}O_5$ $[M+H]^+$ 237.0758, found 237.0756; IR (ν, cm^{-1}): 3315 *br*, 1692, 1634, 1261; ^1H NMR (200 MHz, CD_3OD) δ (ppm): 2.25 (s, 6 H), 7.02 (s, 1 H, CH of enol form), 7.65 (s, 2 H); ^{13}C NMR (50 MHz, CD_3OD) δ (ppm): 16.67, 98.53, 125.87, 127.46, 130.20, 160.87, 165.41, 169.08, 191.99.

1-(2,5-dicyclohexylphenyl)ethanone (4a): $C_{20}H_{28}O$, M_r = 284.44, white powder (2.12 g, 75%), mp = 88–90 °C, ESI-MS:

Calculated for $C_{20}H_{29}O$ $[M+H]^+$ 285.2213, found 285.2206; ^1H NMR (200 MHz, CD_3OD) δ (ppm): 1.43 (m, 12 H), 1.88 (m, 8 H), 2.54 (m, 1 H), 2.60 (s, 3 H), 3.02 (m, 1 H), 7.16 (*d*, *br*, 1 H), 7.30 (*d*, *br*, 1 H), 7.32 (s, 1 H).

(*Z*)-4-(2,5-dicyclohexylphenyl)-2-hydroxy-4-oxobut-2-enoic acid (12): $C_{22}H_{28}O_4$, M_r = 356.46, white powder (1.30 g, 64%), mp. = 146–148 °C, dcc (crystallized from AcOEt/hexane), ESI-MS: Calculated for $C_{22}H_{29}O_4$ $[M+H]^+$ 357.2060, found 357.2062, IR (ν, cm^{-1}): 2976 *br*, 1722, 1630, 1264; ^1H NMR (200 MHz, $CDCl_3$) δ (ppm): 1.29–1.34 (m, 2 H), 1.36–1.45 (m, 8 H), 1.75 (*d br*, 2 H), 1.78 (m, 8 H), 2.51 (m, 1 H), 3.00 (m, 1 H), 3.94 (*s*, CH_2 of diketo form), 6.83 (s, 1 H, CH of enol form), 7.31 (s, 1 H), 7.33 (s, 2 H); ^{13}C NMR (50 MHz, $CDCl_3$) δ (ppm): 26.00, 26.13, 26.76, 26.83, 34.28, 34.68, 40.10, 43.92, 101.38, 127.09, 127.35, 130.75, 134.50, 144.99, 145.62, 163.57, 170.60, 195.05.

4-(2,5-dicyclohexylphenyl)-4-oxobutanoic acid (1a): $C_{22}H_{30}O_3$, M_r = 342.47, white powder (0.92 g, 71%), mp = 122–124 °C, dcc (crystallized from PhMe); ESI-MS: Calculated for $C_{22}H_{31}O_3$ $[M+H]^+$ 343.2268, found 343.2260; ^1H NMR (200 MHz, DMSO-d_6) δ (ppm): 1.32 (*m*), 1.75 (*m*), 2.57 (m, 3 H), 2.93 (m, 1 H), 3.06 (*t*, *J* = 5.62, 12.36 Hz), 3.21 (*t*, *J* = 5.62, 12.36 Hz), 7.10 (*d*, *J* = 7.86 Hz), 7.23 (*s*), 7.28 (*s*), 7.36 (*d*, *J* = 8.42 Hz), 7.51 (*d*, *J* = 7.86 Hz), 7.90 (*d*, *J* = 8.42 Hz), 12.16 (*s*, *br*). Two forms are visible in solution, ratio 8:5 calculated according to the signals of aromatic H-atoms. We assumed the presence of two conformers in solution.

(*Z*)-2-hydroxy-4-(2-methoxyphenyl)-4-oxobut-2-enoic acid (13): $C_{11}H_{12}O_4$, M_r = 208.21, white powder (2.54 g, 70%), mp = 129–131 °C (crystallized from EtOH), ESI-MS: Calculated for $C_{11}H_{11}O_5$ $[M+H]^+$ 223.0601, found 223.0600; IR (ν, cm^{-1}): 2998 *br*, 1711, 1634, 1259; ^1H NMR (200 MHz, DMSO-d_6) δ (ppm): 3.90 (s, 3 H), 4.35 (*s*, *br*, CH_2 of diketo form), 7.08 (*t*, *J* = 7.30, 15.16 Hz, 1 H), 7.13 (s, 1 H, CH of enol form), 7.20 (d, *J* = 7.86 Hz, 1 H), 7.59 (*dt*, *J* = 7.30, 15.72 Hz, 1.68 Hz, 1 H), 7.78 (*dd*, *J* = 7.86, 1.68 Hz, 1 H); ^{13}C NMR (50 MHz, DMSO-d_6) δ (ppm): 53.87, 56.06, 102.76, 112.79, 120.88, 124.12, 130.13, 135.18, 158.91, 163.53, 170.14, 189.72.

(*Z*)-2-hydroxy-4-(3-methoxyphenyl)-4-oxobut-2-enoic acid (14): $C_{11}H_{10}O_5$, M_r = 222.19, white powder (2.64 g, 67%), mp = 139–140 °C (crystallized from EtOH), ESI-MS: Calculated for $C_{11}H_{11}O_5$ $[M+H]^+$ 223.0601, found 223.0602; IR (ν, cm^{-1}): 3256 *br*, 1687, 1626, 1258; ^1H NMR (200 MHz, DMSO-d_6) δ (ppm): 3.83 (s, 3 H), 4.54 (*s*, *br*, CH_2 of diketo form), 7.03 (s, 1 H, CH of enol form), 7.24 (*dd*, $J_{1,3}$ = 7.86 Hz, $J_{1,2}$ = 2.25 Hz, 1 H), 7.46 (t, *J* = 7.86 Hz, 1 H), 7.48 (s, 1 H, overlapped with *t* at 7.46 ppm), 7.62 (d, *J* = 7.86 Hz, 1 H); ^{13}C NMR (50 MHz, DMSO-d_6) δ (ppm): 53.14, 55.47, 98.15, 112.15, 120.14, 120.42, 130.35, 136.29, 159.74, 163.34, 170.78, 189.88.

(*Z*)-4-(3-bromophenyl)-2-hydroxy-4-oxobut-2-enoic acid (15): $C_{10}H_7BrO_4$, M_r = 271.06, white powder (3.35 g, 68%), mp = 143–144 °C (crystallized from EtOH/PhMe), ESI-MS: Calculated for $C_{10}H_6BrO_4$ $[M-H]^-$ 268.9455, found 268.9453; IR (ν, cm^{-1}): 3524, 1628, 1301, 1237; ^1H NMR (200 MHz, DMSO-d_6) δ (ppm): 4.57 (*s*, *br*, CH_2 of diketo form), 7.08 (s, 1 H, CH of enol form), 7.49 (t, *J* = 7.86 Hz, 1 H), 7.85 (*dd*, $J_{1,2}$ = 7.86 Hz, $J_{1,3}$ = 2.25 Hz, 1 H), 8.03 (d, *J* = 8.42 Hz, 1 H), 8.14 (s, 1 H); ^{13}C NMR (50 MHz, DMSO-d_6) δ (ppm): 49.24, 97.64, 122.56, 127.02, 130.31, 131.33, 136.54, 136.97, 163.18, 170.43, 188.79.

(*Z*)-2-hydroxy-4-oxo-4-(3-(trifluoromethyl)phenyl)but-2-enoic acid (16): $C_{11}H_7F_3O_4$, M_r = 260.17, white powder (0.62 g, 61%), mp = 135–137 °C (crystallized from AcOEt/PhMe), ESI-MS: Calculated for $C_{11}H_8F3O_4$ $[M+H]^+$ 261.0369, found 261.0373; IR (ν, cm^{-1}): 3439 *br*, 1673, 1622, 1228; ^1H NMR (200 MHz, $CDCl_3$) δ (ppm): 7.10 (s, 1 H, CH of enol form), 7.20 (s, 1 H, CH of second enol form), 7.67 (*dt*, *J* = 7.86 Hz, 1 H), 7.87 (dd, *J* = 7.86 Hz, 1 H), 8.24 (*s br*, 1 H), 8.18 (d, *J* = 7.86 Hz, 1 H); ^{13}C NMR (50 MHz, $CDCl_3$) δ (ppm): 96.07, 98.13, 124.83, 124.91, 129.79, 129.91, 130.25, 130.32, 130.54, 130.61, 131.10, 134.30, 135.72, 161.91, 162.53, 170.39, 174.75, 185.76, 189.11.

(*Z*)-2-hydroxy-4-oxo-4-(4-(pyrrolidin-1-yl)phenyl)but-2-enoic acid (17): $C_{14}H_{15}NO_4$, M_r = 261.27, red powder, mp = 160–162 °C (crystallized from EtOH/PhMe), ESI-MS: Calculated for $C_{14}H_{16}NO_4$ $[M+H]^+$ 262.1074, found 262.1063; IR (ν, cm^{-1}): 3155 *br*, 1716, 1599, 1272; ^1H NMR (200 MHz, $CDCl_3$/DMSO-d_6) δ (ppm): 2.06 (*qn*, *J* = 6.18 Hz, 4 H), 3.40 (t, *J* = 6.18 Hz, 4 H), 6.56 (d, *J* = 8.99 Hz, 2 H), 7.02 (s, 1 H), 7.89 (d, *J* = 8.99 Hz, 2 H); ^{13}C NMR (50 MHz, $CDCl_3$/DMSO-d_6) δ (ppm): 25.22, 47.54, 97.54, 111.25, 121.39, 130.52, 151.84, 164.61, 165.96, 189.61.

(*Z*)-2-hydroxy-4-(4-morpholinophenyl)-4-oxobut-2-enoic acid (18): $C_{14}H_{15}NO_5$, M_r = 277.27, pale orange powder, mp = 164–165 °C (crystallized from EtOH/PhMe), ESI-MS: Calculated for $C_{14}H_{16}NO_5$ $[M+H]^+$ 278.1023, found 278.1019. IR (ν, cm^{-1}): 3320 *br*, 1713, 1604, 1268; ^1H NMR (200 MHz, D_2O) δ (ppm): 3.35 (t, *J* = 5.05 Hz, 4 H), 3.85 (t, *J* = 5.05 Hz, 4 H), 3.92 (*s*, CH_2 of diketo form), 6.88 (d, *J* = 8.99 Hz, 2 H), 7.01 (s, 1 H), 7.93 (d, *J* = 8.99 Hz, 2 H), 15.64 (*sb*, 1 H); ^{13}C NMR (50 MHz, $CDCl_3$) δ (ppm): 47.21, 53.19, 66.57, 97.90, 113.39, 124.96, 130.37, 154.96, 163.35, 167.19, 190.04.

(*Z*)-4-(4-(1*H*-imidazol-1-yl)phenyl)-2-hydroxy-4-oxobut-2-enoic acid (19): $C_{13}H_{10}N_2O_4$, M_r = 258.23, pale yellow solid, mp = 184–186 °C (crystallized from AcOEt/PhMe), ESI-MS: Calculated for $C_{13}H_{11}N_2O_4$ $[M+H]^+$ 259.0713, found 259.0722; IR (ν, cm^{-1}): 3452 *br*, 1710, 1608, 1277; ^1H NMR (200 MHz, $CDCl_3$) δ (ppm): 7.10 (s, 1 H), 7.27 (m, 1 H), 7.38 (m, 1 H), 7.56 (d, *J* = 8.99 Hz, 2 H), 7.99 (s, 1 H), 8.14 (d, *J* = 8.42 Hz, 2 H); ^{13}C NMR (50 MHz, $CDCl_3$) δ (ppm): 98.07, 117.76, 121.06, 130.09, 131.43, 133.68, 135.49, 141.40, 162.66, 169.81, 189.18.

(*Z*)-2-hydroxy-4-(4-(4-methylpiperazin-1-yl)phenyl)-4-oxobut-2-enoic acid (20): $C_{15}H_{18}N_2O_4$, M_r = 290.31, pale yellow powder, mp = 162–163 °C (crystallized from EtOH/PhMe); ESI-MS: Calculated for $C_{15}H_{19}N_2O_4$ $[M+H]^+$ 291.1339, found 291.1347. IR (ν, cm^{-1}):3420 (*br*), 1645, 1599, 1247; ^1H NMR (200 MHz, DMSO-d_6) δ (ppm): 2.78 (s, 3 H), 3.33 (*m*, *br*, overlapped with residual water signal from solvent), 4.44 (*s*, CH_2 of diketo form), 7.03 (s, 1 H, CH of enol form), 7.10 (d, *J* = 9.0 Hz, 2 H), 7.98 (d, *J* = 9.0 Hz, 2 H), 11.42 (*s br*, 1 H); ^{13}C NMR (50 MHz, DMSO-d_6) δ (ppm): 40.77, 41.86, 43.66, 51.62, 97.43, 114.03, 124.35, 130.27, 153.44, 163.53, 168.20, 189.64.

(*Z*)-4-(4-(dimethylamino)phenyl)-2-hydroxy-4-oxobut-2-enoic acid (21): $C_{12}H_{13}NO_4$, M_r = 235.24, pale red solid, mp = 155–157 °C (crystallized from EtOH/PhMe); ESI-MS: Calculated for $C_{12}H_{14}NO_4$ $[M+H]^+$ 236.0917, found 236.0918. IR (ν, cm^{-1}): 3382 *br*, 1719, 1602, 1274. ^1H NMR (200 MHz, CD_3OD) δ (ppm): 3.10 (s, 6 H), 6.78 (d, *J* = 8.99 Hz, 2 H), 7.01 (s, 1 H), 7.91 (d, *J* = 8.99 Hz, 2 H); ^{13}C NMR (50 MHz, CD_3OD) δ (ppm): 40.10, 98.19, 112.26, 123.02, 131.44, 155.98, 165.72, 168.36, 191.03.

The CAS numbers for already reported compounds are: 113416-61-8 for **1**; 1224740-28-6 for **2**; 1224740-52-6 for **3**; 1224740-57-1 for **4**; 149281-53-8 for **5**; 1799810-91-5 for **6**; 1799810-93-7 for **7**; 1799811-01-0 for **8**; 1207167-72-3 for **9**; 1799811-06-5 for **10**; 760207-27-0 for **13**; 868616-56-2 for **14**; 260558-95-0 for **15**; 1224740-53-7 for **16**; 1799811-04-3 for **17**; 927904-77-6 for **18**; 1224739-86-9 for **19**; 1146317-98-7 for **22**; 1207167-69-8 for **23**; 1207167-70-1 for **24**; 1207167-71-2 for **25**; 160428-91-1 for **26**; 36330-85-5 for **3a**; 2234-14-2 for **5a**.

The full characterization of compounds **8**, **10** and **17** is, for the first time, given in this manuscript.

2.1.1. Antibacterial activity

Bacterial Strains. Antimicrobial susceptibility testing control organisms *Escherichia coli* NCTC 12241, *Staphylococcus aureus* (NCTC *12981* and NCTC *13373*), *Enterococcus faecalis* NCTC *12697* and *Bacillus subtilis* NCTC 10400 were obtained from the National Collection of Type Cultures (Public Health England, UK). Tetracycline-resistant MRSA isolate XU212 (expressing a TetK efflux

pump) was obtained from Dr. E. Udo [11]. Erythromycin-resistant *S. aureus* RN4220 was provided by Dr. Jonathan Cove [12]. EMRSA-15 [13] was from the culture collection of Dr. Paul Stapleton. Norfloxacin-resistant *S. aureus* 1199B, which over-expresses the NorA efflux pump, was kindly donated by Professor Glenn W. Kaatz [14].

Minimum inhibitory concentration (MIC) determination. MICs were determined by the microdilution method [15] in 96-well microtitre plates in a total volume of 200 μL per well. The growth medium used was cation-adjusted (20 mg/l Ca^{2+} and 10 mg/L Mg^{2+}) Mueller-Hinton broth (Oxoid, UK) with a bacterial inoculum of 5×10^5 colony-forming units per milliliter. Plates were incubated at 37 °C and read by visual inspection after 16 h. The MIC was recorded as the lowest concentration that inhibited visible growth within the time period. All compounds were prepared in DMSO and diluted such that the solvent was less than 1% in well of the microtitre plate. DMSO concentrations 5% or less has previously been demonstrated not to affect growth of the organisms assessed (unpublished observation). Compounds were evaluated within the range 0.12–128 μg/ml and MICs were determined at least twice. MIC values were converted into molar units (μmol/L), and such values were input for SAR study.

2.1.2. Molecular similarity

Structural similarity between compounds studied and fluoroquinolone antibiotics was calculated by overlapping conformational assembly of each ADK with the structure of norfloxacin as a template molecule, using Openeye ROCS program [16]. Degree of overlap was quantified using Tanimoto scoring function [17].

2.1.3. 3D QSAR study

In order to correlate antibacterial activity with the structure of compounds, we made 3D QSAR model using Pentacle 1.06 software. As a dependent variable, we have chosen potencies toward norfloxacin-resistant *S. aureus* 1199B, expressed as −log(MIC). For each ADK, a set of conformers was generated in OMEGA 2.4.3 [18] using a MMFF94s force field [19]. In order to simulate appropriate ionization state under physiological conditions, compounds were modeled as carboxylates (monoanionic form). Structures were additionally optimized using semiempirical PM6 method [20] implemented in MOPAC 2016 [21].

Molecular interaction fields (MIFs) [22] were calculated using four GRID probes: DRY which represents hydrophobic interactions, O is sp^2 carbonyl probe which maps H-bond donor features of molecules; N1 is neutral flat −NH probing H-bond acceptors in molecules, and TIP probe introduces the shape of molecules in model building [23]. Pentacle software computes alignment-independent descriptors (GRIND-2 descriptors) where each variable represents the product of the most favorable interaction energies (IE) of two GRID probes in a given distance range. The majority of 3D-QSAR programs like CoMFA [24] and CoMSIA [25] require spatial alignment of structures before MIF computation, and since there are no strict criteria for alignment, results are strongly affected by the quality of the alignment. Alignment-independent methods like GRIND overcome the problem with alignment and this method is widely used in SAR research [26–29].

Important positions around molecules (hot spots) are extracted from MIFs using AMANDA discretization algorithm [30]. Encoding of the filtered MIFs into GRIND variables was performed by the maximal auto- and cross-correlation (MACC2) algorithm. The weight of GRIND correlograms that encode DRY probe is increased by changing its cut-off value from −2.8 (default) to −2. All other parameters for MIF computation were retained at default values. GRIND variables are correlated with antibacterial activity using partial least square (PLS) method [31].

2.1.4. Molecular docking

In order to elucidate potential bacterial proteins targeted by ADKs, docking studies were performed. Targets were chosen according to literature data, and Pharmmaper [32] searches for the two most potent derivatives. The following proteins were selected as putative targets from *S. aureus*: DNA gyrase and dehydrosqualene synthase (CrtM). Furthermore, additional bacterial targets were selected from *E. coli* (undecaprenyl diphosphate synthase (UPSS), methionine aminopeptidase (MetAP) and β-lactamase), *K. pneumoniae* (β-lactamase) and *S. enterica* (tryptophan synthase). These targets are also present in the strains that were used in the *in vitro* testing and were considered for molecular docking studies without homology modeling. The information of Protein Data Bank (PDB) codes used for retrieving the experimental structures is given in Table 6. After removal of ligand and water molecules hydrogen atoms were added, and proteins were neutralized through the addition of sodium or chloride ions and embedded in the water box. Solvated proteins were minimized by keeping the protein backbone, DNA backbone (for 2XCT) and metal ions fixed to preserve the experimental structure. The 10 ps conjugate gradient minimization was performed in NAMD 2.12 program, using CHARM force field. AutoDock Vina software was used for docking. Exhaustiveness was set to 15, and only the most favorable binding mode was calculated for each molecule. Raising the exhaustiveness to 250 gave the same results for docking against the 4H3A as a target.

The.sdf database consisting of ADKs in monoanionic and dianionic form as well, and compounds **1a**-**5a** were prepared, starting from the best-ranking conformation generated with OMEGA 2.5.1.4 software, and further optimized using semiempirical PM7 method implemented in MOPAC 2016. Vega ZZ software was used as a GUI for all calculations. Images of docking solutions were prepared using BIOVIA Discovery Studio 2016.

2.1.5. HSA binding experiments

Fatty acid-free human serum albumin (HSA, <0.007% fatty acids, Mw = 66478 Da) was purchased from Sigma, as well as potassium dihydrogen phosphate, disodium hydrogen phosphate, sodium chloride and potassium chloride used for PBS preparation. A stock solution of HSA ($c = 1.96 \times 10^{-4}$ M) was prepared by dissolving accurately weighted mass of commercially available lyophilized HSA in freshly prepared 30 mM PBS (pH 7.38). A stock solution of 2,5-di-cyclohexyl ADK ($c = 1.63 \times 10^{-3}$ M) was prepared by dissolving a substance in DMSO, because of its low solubility in the buffer. For HSA-ADK interaction studies, HSA solution was freshly prepared from the stock by dilution with a buffer (HSA concentration was kept constant, $c = 5 \times 10^{-7}$ M), and titrated with small volume increments of ADK stock solution, to avoid large sample dilution. ADK was added in 0.5, 1, 1.5, 2, 3, 4, 6 and 8 molar equivalents. After each aliquot addition, the system was stirred and left to equilibrate for 20 min before UV/Vis absorption and fluorescence emission spectra recording. At the end of the titration (8 equivalents of substance added) the final DMSO volume did not exceed 2%. It was shown that addition of 15% of DMSO did not induce structural changes in bovine serum albumin (BSA), a protein structurally similar to HSA [33]. Therefore, it is unlikely that the conformation of HSA was changed with the level of DMSO used in this study. Millipore water was used for buffer solution preparation.

Fluorescence measurements were performed on spectrofluorometer Fluoromax-4 Jobin Yvon (Horiba Scientific, Japan), equipped with Peltier element for temperature control and magnetic stirrer for cuvette, using quartz cell with 1 cm path length and 4 ml volume. Before the fluorescence spectra recording, diluted HSA solution was filtrated using 0.22 μm pore size filters. An excitation wavelength was 280 nm, with 5 nm slits; emission spectra were

recorded in 300–450 nm wavelength range, with 5 nm slits, and 0.1 s integration time. Background PBS signal was subtracted from each spectrum.

UV/Vis spectra were recorded on a GBC Cintra6 UV/Vis spectrophotometer, using quartz cell with 1 cm path length and 4 ml volume. All spectra were recorded against the corresponding blank (PBS) in 250–450 nm wavelength range at room temperature.

2.1.6. Acidity constant (pK_a value) determination

Acidity constant (pK_{a2} value) of compound **12** was determined using spectrophotometric titration at $t = 20 \pm 0.5$ °C. Working solution ($c_{\mathbf{12}} = 5 \times 10^{-5}$ M) was prepared by dissolving an accurately weighed substance in 2.50 ml of ethanol, 10 mM phosphate buffer (pH = 10.44, I = 0.1 M (NaCl)) was added up to 100.00 ml. Increments of concentrated or 1 M H_3PO_4 were added stepwise to reach pH~4 when precipitation occurred (total volume change at the end of the titration was lower than 2%). pH Value was continuously measured during titration and UV/Vis spectra recorded after solution pH value equilibration. UV/Vis spectra were recorded on GBC Cintra6 UV/Vis spectrophotometer, using quartz cell with 1 cm path length and 4 ml volume. All spectra were recorded against the corresponding blank in 210–600 nm wavelength range. Three sets of experiments were performed. Acidity constant value (K_{a2}) was determined according to transformed form of classical spectrophotometric equation: [34].

$$A = A_{A^{2-}} + \frac{1}{K_{a2}}[H_3O^+](A_{HA^-} - A) \quad (1)$$

where A_{HA^-}, A_{A2-}, and A represent absorbances of monoanionic (HA^-), dianionic (A^{2-}) forms of **12** and their mixture at specified wavelengths, respectively. Equation (1) gave linear dependence where the spectrum of only one "pure" form (HA^-) was needed for K_{a2} determination. K_{a2} Value was calculated by linear regression analysis from the slope of corresponding fitting line, (results are shown as an average value ± 95% confidence interval).

pH Values were measured using CRISON pH-Burette 24 2S equipped with CRISON 50 29 micro-combined pH electrode (CRISON INSTRUMENTS, S.A. Spain). The electrode was calibrated by standard CRISON buffer solutions (pH 4.01, 7.00, and 9.21).

2.1.7. Shake-flask logD determination

Standard shake-flask method was used for log$D$ (pH 7.4, 10 mM phosphate buffer) determination [35,36]. Stock solution of compound **12** ($c_{\mathbf{12}} = 5.0 \times 10^{-3}$ M) was prepared in octanol saturated with buffer. Octanol/buffer volume ratio was set according to estimated log$D$ (pH 7.4) value; MarwinSketch (www.chemaxon.com) was used for log$D$ value estimation.

The concentration of compound **12** in aqueous phase was determined spectrophotometrically using a calibration curve method. Due to a low octanol volume used, concentration of **12** in octanol phase was determined as a difference between total and aqueous phase compound **12** concentration. Three octanol/buffer volume ratios were used for the experiment and the result is given as a mean ± 95% confidence interval.

3. Results

3.1. Antibacterial activity

The antibiotic activity of ADK against Gram-positive MDR strains was reported for the first time in our previous study, and two congeners had a comparable activity with norfloxacin. The analogues with the 2,4-di-iPr and 2,4,6-tri-Et substitutions on the aromatic ring exerted broad spectrum activity [6]. The molecular field interactions analysis indicated the importance of DRY-DRY and DRY-N1 variables for the activity of these compounds. Furthermore, we postulated that the keto-enol moiety is responsible for the antibacterial activity.

Therefore, we have designed a series of new congeners by systematic introduction of bulky hydrophobic substituents at different positions in the aromatic ring. An additional set of congeners with small hydrophobic or small polar substituents on the aromatic ring and congeners without keto-enol moiety were selected for synthesis and testing, for the comparison.

As anticipated, several compounds (Table 1) were found to have activity against MDR Gram-positive (G+) organisms, *Enterococcus faecalis*, *Bacillus subtilis* and *Staphylococcus aureus*. As predicted by rational design, compound **12** exhibited notable activity against *E. faecalis*, and *S. aureus*, including both methicillin-susceptible and -resistant isolates. Compound **12** was 10 times more potent toward SA 1199B strain than compound **25**, the most potent ADK from previously studied set of ADK, [6], and also 10 times more potent than norfloxacin against the same bacterial strain. None of the compounds were active against the Gram-negative (G−) organism *Escherichia coli* (MICs >128).

ADKs are good chelators of Mg^{2+} [39] and keto-enolic moiety is involved in interaction with a metal ion. Since prenyl-transferases with the Mg^{2+}/Asp motif in the active site, are identified as possible targets for ADK in a bacterial cell, we wanted to check whether ADK metal complexation ability influences their potency toward MDR bacterial strains. Antibacterial activities of two sets of compounds, comprising three phenyl-substituted aroylpropanoic acids (**1a**-**3a**) and two acetophenones (**4a**, **5a**) (Fig. 4), were tested (Table 1). Potencies of compounds lacking diketo moiety (**1a**-**5a**) are notably lower compared to the ADKs with the same phenyl substituent pattern. This result is in line with a hypothesis that metal complexation ability is important for the antibacterial activity of ADKs.

The most potent compounds were also tested on human MRC-5 cell lines, and showed notable cytotoxicity: IC_{90} (compound **9**) ~ 90 μM, IC_{90} (compound **12**) ~ 30 μM. It is important to note that the most potent compounds show selectivity toward bacterial *vs*. human cells in some extent, but further structural modifications would be necessary to increase the selectivity.

3.2. Molecular similarity between ADK and norfloxacin

In our previous study of ADKs' antibacterial activities, structure similarity between ADK and norfloxacin was examined. It was previously shown in a qualitative manner that the better overlap of structures corresponds to the more potent derivatives [6]. A quantitative evaluation of molecular similarity was carried out for the set of molecules in this study. It was noticed that the most potent ADK derivatives show the best shape complementarity with norfloxacin, as seen from ROCS Overlap Function. However, pharmacophoric similarity between the most potent ADK and norfloxacin was the smallest, as seen from the Color Tanimoto scores (Table 2). One may assume that the mechanism of antibacterial action of ADK with bulkier phenyl substituents is different from the norfloxacin (inhibition of topoisomerase II and IV and prevention of cell division).

3.3. QSAR

3.3.1. PCA model

Principal component analysis (PCA) is performed on the whole set of GRIND descriptors. 5 PC model explained 84.45% of X sum of squares (SSX_{acc}), and 76.43% of X variance ($VarX_{acc}$). In order to reduce number of variables, one cycle of fractional factorial design

Table 1
Structure and antibacterial activities of ADKs (compounds **1**–**26** including previously reported activities for compounds **1** and **22**–**26**), compounds without diketo moiety (**1a**-**5a**, see Fig. 4) and antibiotics (**norfloxacin**, **ciprofloxacin**, **levofloxacin**, **moxifloxacin**) against several bacterial strains. Minimal inhibition concentrations (MIC) which inhibited bacterial growth are given in μM.

Comp.	R-	*E.faecalis* NCTC 12697	*B.subtilis* NCTC 10400	*S. aureus* NCTC 12981 (MSSA)	SA-NCTC 13373 (MRSA)	SA- 1199B	SA RN4220	SA EMRSA-15	SA XU212
1	H	*n.d.*	*n.d.*	*n.d.*	*n.d.*	>2660	*n.d.*	*n.d.*	*n.d.*
2	2-Me	–	–	–	–	–	–	–	–
3	3-Me	–	–	–	–	–	–	–	–
4	4-*n*Bu	129	–	258	258	258	258	258	258
5	2,4-di-Me	–	–	–	–	–	–	–	–
6	2,4,5-tri-Me	–	–	–	–	–	–	–	–
7	2,3,5,6-tetra-Me	516	–	–	–	–	–	–	–
8	β-tetralinyl	260	–	–	–	520	–	520	–
9	2,4,6-tri-*i*Pr	–	25	13	–	25	50	25	50
10	4-OMe −2,5-di-Me	–	–	–	–	–	–	–	–
11	4-OH-3,5-di-Me	–	–	–	–	–	–	–	–
12	2,5-di-cyclohexyl	6	125	11	11	11	11	22	11
13	2-OMe	–	–	–	–	–	–	–	–
14	3-OMe	–	–	–	–	–	–	–	–
15	3-Br	–	–	–	–	–	–	–	–
16	3-CF_3	–	–	–	–	–	–	–	–
17	4-pyrrolidinyl	–	–	–	–	–	–	–	–
18	4-morpholinyl	–	–	–	–	–	–	–	–
19	4-imidazolyl	496	496	–	248	124	–	–	496
20	4-*N*-Me piperazinyl	–	–	–	–	–	–	–	–
21	4-*N*,*N*-diMe	–	–	–	–	–	–	–	–
22	4-*t*-Bu	*n.d.*	*n.d.*	*n.d.*	*n.d.*	1030	–	–	–
23	2,4-di-*i*Pr	*n.d.*	*n.d.*	*n.d.*	*n.d.*	232	232	232	464
24	2,5-di-*i*Pr	*n.d.*	*n.d.*	*n.d.*	*n.d.*	232	464	232	464
25	2,4,6-tri-Et	*n.d.*	*n.d.*	*n.d.*	*n.d.*	116	232	232	232
26	4-Ph	*n.d.*	*n.d.*	*n.d.*	*n.d.*	477	–	–	–
1a	2,5-di- cyclohexyl AP	*n.d.*	*n.d.*	94	94	47	47	94	47
2a	2,4,6-tri-*i*Pr AP	*n.d.*	*n.d.*	–	–	–	–	–	–
3a	4-Ph AP	*n.d.*	*n.d.*	–	–	–	–	–	–
4a	2,5-di-Ch A	*n.d.*	*n.d.*	450	450	450	225	225	225
5a	2,4,6-tri-*i*Pr A	*n.d.*	*n.d.*	–	–	–	–	–	–
Norfloxacin [37] [14]		6.3	*n.d.*	*n.d.*	*n.d.*	106	–	3,3	–
Ciprofloxacin [37,38]		1.5	*n.d.*	*n.d.*	*n.d.*	24.2	0.76	*n.d.*	*n.d.*
Levofloxacin [37] [38]		1.4	*n.d.*	*n.d.*	*n.d.*	5.53	0.69	*n.d.*	*n.d.*
Moxifloxacin [38]		*n.d.*	*n.d.*	*n.d.*	*n.d.*	0.62	0.31	*n.d.*	*n.d.*

n.d. – not determined; – inactive (MIC > 128 μg/mL); AP- aroylpropanoic acids; - A-ketone (Fig. 4).

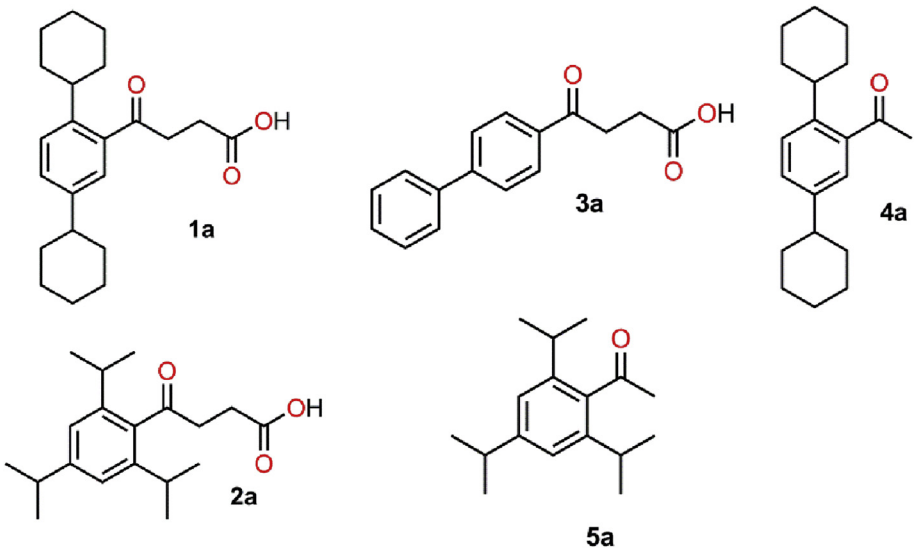

Fig. 4. Structural modifications of ADK lacking diketo (keto-enolic) moiety.

(FFD) is performed and results are shown in Table 3.

Inspection of PCA scores plot (PC2 vs PC1) reveals clustering of compounds into two groups (Fig. 5).

Compounds are clustered according to number of H-bond donors. First cluster, located at the far right of the graph, contains molecules with two H-bond donor (HBD) groups, second cluster groups molecules with one HBD, while compounds **1a** and **4a** are outliers since they have no HBD groups.

Table 2
Tanimoto and ROCS overlap scoring functions for overlaps of ADK with norfloxacin template.

Comp.	Tanimoto Combo	Shape Tanimoto	Color Tanimoto	Overlap	Comp.	Tanimoto Combo	Shape Tanimoto	Color Tanimoto	Overlap
1	0.940	0.635	0.305	644.132	**14**	0.931	0.652	0.279	689.710
2	0.909	0.603	0.306	641.157	**15**	0.937	0.657	0.280	670.207
3	0.958	0.654	0.305	672.227	**16**	0.998	0.694	0.304	757.203
4	0.904	0.615	0.289	691.311	**17**	1.047	0.670	0.376	758.256
5	0.923	0.616	0.306	665.772	**18**	0.993	0.690	0.303	790.267
6	0.918	0.612	0.306	679.306	**19**	0.974	0.667	0.307	766.072
7	0.839	0.564	0.275	661.592	**20**	1.053	0.662	0.391	787.194
8	0.971	0.699	0.273	757.711	**21**	0.948	0.635	0.313	694.573
9	0.793	0.734	0.059	860.108	**1a**	0.846	0.703	0.143	878.132
10	0.844	0.564	0.280	661.289	**2a**	0.886	0.599	0.287	740.503
11	0.953	0.693	0.260	733.759	**3a**	1.064	0.708	0.355	783.744
12	0.805	0.672	0.133	876.715	**4a**	0.976	0.795	0.181	866.392
13	0.891	0.608	0.283	662.311	**5a**	0.735	0.569	0.166	655.108

Table 3
Statistics of the PCA model generated after 1 FFD cycle (out of 490 variables, 272 were retained).

Component	SSX	SSX_{acc}	VarX	VarXacc
1	48.11	48.11	44.29	44.29
2	14.87	62.98	12.82	57.11
3	9.65	72.63	8.47	65.57
4	8.22	80.85	8.09	73.67
5	3.6	84.45	2.76	76.43

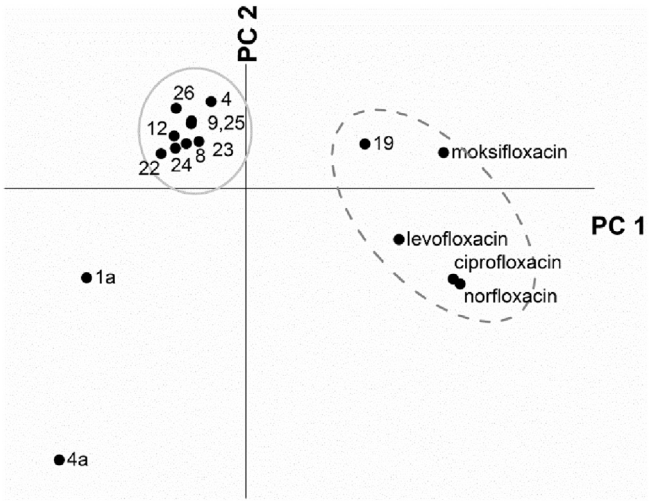

Fig. 5. PCA scores plot of PC2 vs PC1, for all compounds included in 3D QSAR model.

In order to rationalize which structural features of studied compounds contribute to the overall potency, we made partial least square (PLS) model using pMIC (−logMIC) values against SA1199B strain as dependent variable, and the whole set of GRIND descriptors as independent ones. The resulting 2 latent variable (LV) model had $r^2 = 0.88$, q^2 (leave-one-out, LOO cross-validation) = 0.43 and standard deviation of error of prediction (SDEP) = 0.62. The predictivity of model is highly improved by applying one cycle of FFD (2LV, $r^2 = 0.90$, q^2 (LOO) = 0.72 and SDEP = 0.43), which reduced the number of variables from 490 to 272. Besides leave-one-out, leave-two-out (LTO) and random group (RG) cross-validation (CV) procedures are also performed. Splitting of this relatively small set of compounds (16 comp.) to training and test is not done, since random group validation essentially provides the same information on model predictivity. Statistics of models obtained using three CV procedures is shown (Table 4).

The graphs of calculated *vs* experimental (Fig. 6a) and predicted *vs* experimental potency (Fig. 6b) for 2LV model with LOO CV are shown.

The potency of all compounds is predicted within 2 SDEP limit.

PLS coefficients plot (Fig. 7) shows which descriptors have positive or negative impact on potency.

Variables with the highest influence on potency are labeled in Fig. 7, and their association with structural elements of compounds is described in Table 5.

The information obtained from each block of variables are described in following lines:

- DRY-DRY correlograms define optimal distance between two hydrophobic groups. While small distance variables have negative impact on potency, two DRY hot spots at distances from 10 to 16 Å positively contribute to antibacterial activity;
- N1-N1 block of variables is directly correlated with biological activity of compounds, with optimal node-node distance of 11.60–12.00 Å;
- DRY-N1 cross-correlograms define optimal distance between HBA group and non-polar moiety (16.40–16.80 Å). Variables with smaller node-node distances (11.20–11.60 Å) are inversely correlated with potency;
- Variable block O-N1 describes optimal distance between HBD and HBA groups. All variables up to 16.40 Å distance are directly proportional to potency, while larger distances seemed inversely correlated.
- O-TIP correlograms provide the same information as O-N1 variables.

The most relevant variables for antibacterial activity of studied compounds are shown in Fig. 8.

The SAR study on a series of ADK congeners with notable activity against MDR Gram-positive bacteria revealed that two hydrophobic regions at distances from 10 to 16 Å positively influence antibacterial activity. The presence of two HBA groups increases potency, with optimal distance of 11.60–12.00 Å. The optimal

Table 4
Statistics of 2LV PLS model after application of different CV procedures.

Component	SSX_{acc}	SDEC	SDEP	r^2_{acc}	q^2_{acc}
2 LV (LOO)	57.51	0.26	0.43	0.90	0.72
2 LV (LTO)	57.87	0.26	0.46	0.90	0.70
2 LV (RG)	60.33	0.26	0.53	0.90	0.59

FFD-LV = 2, 20% of dummy variables, 20 randomization cycles, 3 random groups.

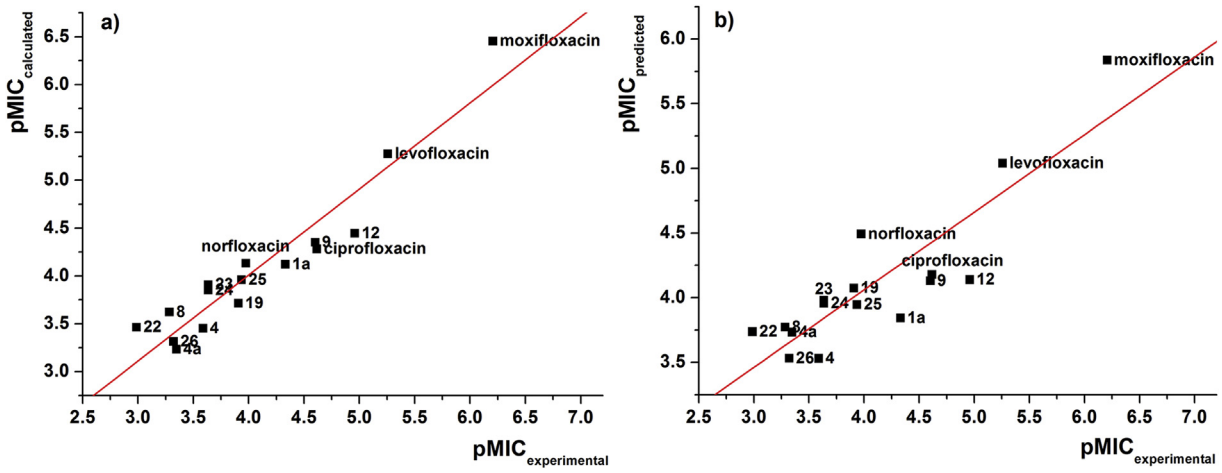

Fig. 6. The graphical representation of: a) calculated *vs* experimental pMIC, and b) predicted *vs* experimental pMIC.

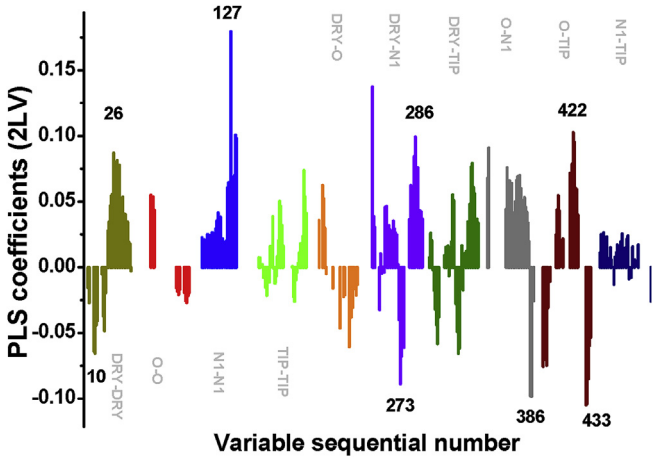

Fig. 7. PLS coefficients plot (2 LV model) showing variables with positive values (positive impact on potency) or negative values (negative impact on potency). More intensive variables means higher influence of corresponding structural features on the potency of compounds. The most important variables are labeled by numbers, and discussed in the text.

distance between hydrophobic moiety and HBA group is found to be 16.40–16.80 Å, and smaller DRY – N1 node distances are linked to decreased potency of compounds. The presence of HBA group at the distance up to 16 Å from HBD positively influences potency, while larger distances are negatively correlated. Steric hot spots, represented through TIP probe, have similar optimal distance from HBD probe (11–14 Å), and nodes at distance larger than 16 Å have negative impact on model. While these ligand based SAR observations provide some guidance for design of novel analogues with improved activity, the structure based design would be needed to improve the selectivity of ADKs towards bacterial targets.

3.4. Molecular docking

Molecular docking was carried out to elucidate potential binding modes with bacterial enzymes and propose a putative target for most active molecules (Table 6). Our previous reported studies indicate that ADK can exist in monoanionic and dianionic forms at physiologically relevant pH, as well as confirmed by our judicious determination and analysis of pK_a values for compound **12** reported further down in the manuscript. Therefore, we have carried out docking using two different forms for all ADK compounds in this study. The docking results suggest that most likely targets in *S. aureus* are dehydrosqualene synthase and DNA gyrase with binding energies over −9 kcal/mol for monoanionic form and even over −10 kcal/mol for dianionic forms. It is apparent that compound **12** in these two targets have a potential to interact with

Table 5
Highlights of variables having highest influence on potency of compounds toward SA1199B.

Probe block	Variable N°	Distance (Å)	Impact	Structural elements, comments
DRY-DRY	10	4.00 −4.40	−	Aromatic ring and another hydrophobic moiety at short distance. More pronounced in less potent compounds
DRY-DRY	26	10.40 −10.80	+	The most potent compounds (12 and moxifloxacin) have the highest variable values (VV). Optimal distance between two hydrophobic groups.
N1-N1	127	11.60 −12.00	+	Only present in the most potent compounds. Represents distance between carboxylate and keto or methoxy group oxygen at given distance.
DRY-N1	273	11.20 −11.60	−	More pronounced in less potent compounds. The smallest VV is for moxifloxacin, differentiating it from norfloxacin, ciprofloxacin and levofloxacin. Compounds **9** and **12** also have small VV.
DRY-N1	286	16.40 −16.80	+	Optimal distance between HBA and hydrophobic group. More pronounced in more potent compounds, with highest VV for moxifloxacin.
O-N1	386	17.20 −17.60	−	Large distance between HBA (carboxylate) and protonated nitrogen atom of norfloxacin, ciprofloxacin and **19**. Not present in most potent compounds.
O-TIP	422	12.00 −12.40	+	More pronounced in more potent compounds. Complementary to O-N1 variable block at smaller node-node distances.
O-TIP	433	16.40 −16.80	−	HBD group relatively far from steric hot spot. Only expressed in less potent compounds. Provides the same information as variable 386.

Table 6
The docking scores of the best-docked compounds into the several bacterial target proteins.

Target	PDB code	Compounds docked as monoanions		Compounds docked as dianions	
		Compounds with the most favorable binding energies (values given in brackets in kcal/mol)	Binding energy range for all compounds (kcal/mol)	Compounds with the most favorable binding energies (values given in brackets)	Binding energy range for all compounds (kcal/mol)
S. aureus CrtM	4F6V	**23**, **12**, **1a** (−9.9, −9.7, −9.7)	−9.9 to −7.2	**12**, **23**, **26** (−10.6, −9.9, −9.9)	−10.6 to −7.8
S. aureus DNA gyrase	2XCT	**12**, **1a**, **4a** (−9.6, −8.8, −8.8)	−9.6 to −6.4	**12**, **23**, **20** (−9.6, −9.2, −8.7)	−9.6 to −7.1
E. coli MetAP	1C21	**12**, **1a**, **4a** (−8.5, −7.5, −7.1)	−8.5 to −5.5	**12**, **24**, **8** (−8.1, −6.8, −6.7)	−8.1 to −5.6
E. coli UPPS	4H3A	**12**, **1a**, **26** (−7.7, −7.4, −7.3)	−7.7 to −5.5	**12**, **26**, **4** (−8.0, −7.6, −7.4)	−8.0 to −6.0
E. coli serine β-lactamase	4LEN	**16**, **8**, **22** (−6.0, −5.8, −5.7)	−6.0 to −4.6	**8**, **22**, **16** (−6.1, −5.9, −5.9)	−6.1 to −4.9
K. pneumoniae β-lactamase	1RCJ	**12**, **1a**, **4a** (−8.3, −8.2, −7.9)	−8.3 to −6.2	**12**, **8**, **7** (−8.4, −8.0, −7.8)	−8.4 to −6.7
S. enterica tryptophan synthase	1QOP	**1a**, **12**, **26** (−8.1, −8.0, −7.8)	−8.1 to −5.6	**12**, **26**, **8** (−8.3, −8.0, −7.7)	−8.3 to −6.0

UPPS- Undecaprenyl diphosphate synthase; MetAP - Methionine aminopeptidase. CrtM - Dehydrosqualene synthase.

positively charged ions (Mn^{2+} and Mg^{2+}), confirming our hypothesis that ADK − metal ion interactions may play an important role for their activity. Albeit the binding mode for two different ionic forms appear different in the docking poses in the CrtM binding site (Fig. 9), their importance for the inhibitory activity for this enzyme may be similar. Furthermore, our most active compound may form interactions with other important enzymes in the bacterial life cycle, including UPPS interacting in a similar binding mode as the ADK with a large hydrophobic moiety reported in Ref. [8]. This provides an opportunity for designing a molecule that is multi-targeting and could effectively inhibit resistant pathways, and offer a more effective approach against infectious diseases [40].

3.5. Physico-chemical profiling of compound 12

3.5.1. HSA binding

Human serum albumin (HSA) is the major soluble and the most versatile transport protein in blood circulation with plenty of physiological functions. HSA contributes significantly to colloidal osmotic pressure and aids the transport, distribution and metabolism of many endogenous and exogenous ligands, with particular affinity to hydrophobic, negatively charged molecules [41]. Therefore, knowledge of binding properties of potential drug molecule to HSA is crucial in drug design and development. HSA binding of **12** was investigated using fluorescence spectroscopy and molar ratio method for stability constants determination.

The changes in HSA emission spectrum at $T = 303$ K upon addition of compound **12** are given in Fig. 10 (changes in HSA emission spectra upon addition of **12,** recorded at 293 and 310 K, are given in Supplementary material, Fig. S26). Decrease of HSA fluorescence intensity (fluorescence quenching) is observed during titration at all temperatures, with the blue shift of emission maxima. Large blue shift indicates the formation of HSA-ADK complex, leading to more hydrophobic microenvironment around fluorescent residue Trp214.

With the increasing amount of quencher, results may deviate from the linearity due to instrumental inner filter effect. This effect can be removed using Lakowicz equation (2):

$$F_{corr} = F_{obs} \times 10^{\frac{A_{ex}+A_{em}}{2}} \quad (2)$$

where F_{corr} and F_{obs} are corrected and observed fluorescence intensities, and A_{ex} and A_{em} are absorbancies at the excitation and emission wavelengths, respectively [42]. Since absorbancies at both, excitation and emission, wavelengths did not exceed 0.05 in all measurements, we used raw data for further calculations.

Fluorescence quenching data were processed using Stern-Volmer (S-V) equation (3):

$$\frac{F_0}{F} = 1 + K_{sv}[Q] = 1 + K_q\tau_0[Q] \quad (3)$$

where F_0 and F represents HSA fluorescence intensities in absence (F_0) and presence of quencher (F), K_{sv} and K_q are S-V's quenching constant and the quenching rate constant of protein, respectively; τ_0 is the average fluorescence lifetime (7.09 ns for HSA) [43] and [Q] is the concentration of the quencher (comp. **12**). The plot of F_0/F *vs.* [Q] at three temperatures is shown in Fig. 11, and results of linear regression analysis are shown in Table 7.

Linearity of S-V plots indicates single quenching mechanism for all compound/HSA ratios.

Fluorescence quenching mechanism is classified as static or dynamic. One way to resolve the quenching mechanism is the evaluation of binding constants' temperature dependence. Dynamic quenching is highly dependent upon diffusion. Higher temperatures result in faster diffusion and hence larger values for biomolecular quenching constant. On the other hand, higher temperatures will typically result in the dissociation of weakly bound complexes, and therefore decrease the biomolecular quenching constant in static process. K_{sv} Value decreases as temperature increases (Table 7), indicating static quenching mechanism. Another confirmation of static quenching mechanism is the value of K_q, which is significantly higher than the maximum scatter collision quenching constant value (2×10^{10} M^{-1} s^{-1}) [44]. The quenching process was further analyzed using modified S-V equation (4):

$$\frac{F_0}{\Delta F} = \frac{1}{f_a K_a}\frac{1}{[Q]} + \frac{1}{f_a} \quad (4)$$

where ΔF is the difference in fluorescence intensity of HSA in the absence (F_0) and in the presence of the quencher at concentration [Q], K_a represents the effective quenching constant for the accessible fluorophores, and f_a is the fraction of accessible fluorophore. The results of linear fit are shown in Fig. 12 and in Table 8.

Results show that the fluorophore (Trp214) is fully accessible to quencher (f_a ~1).

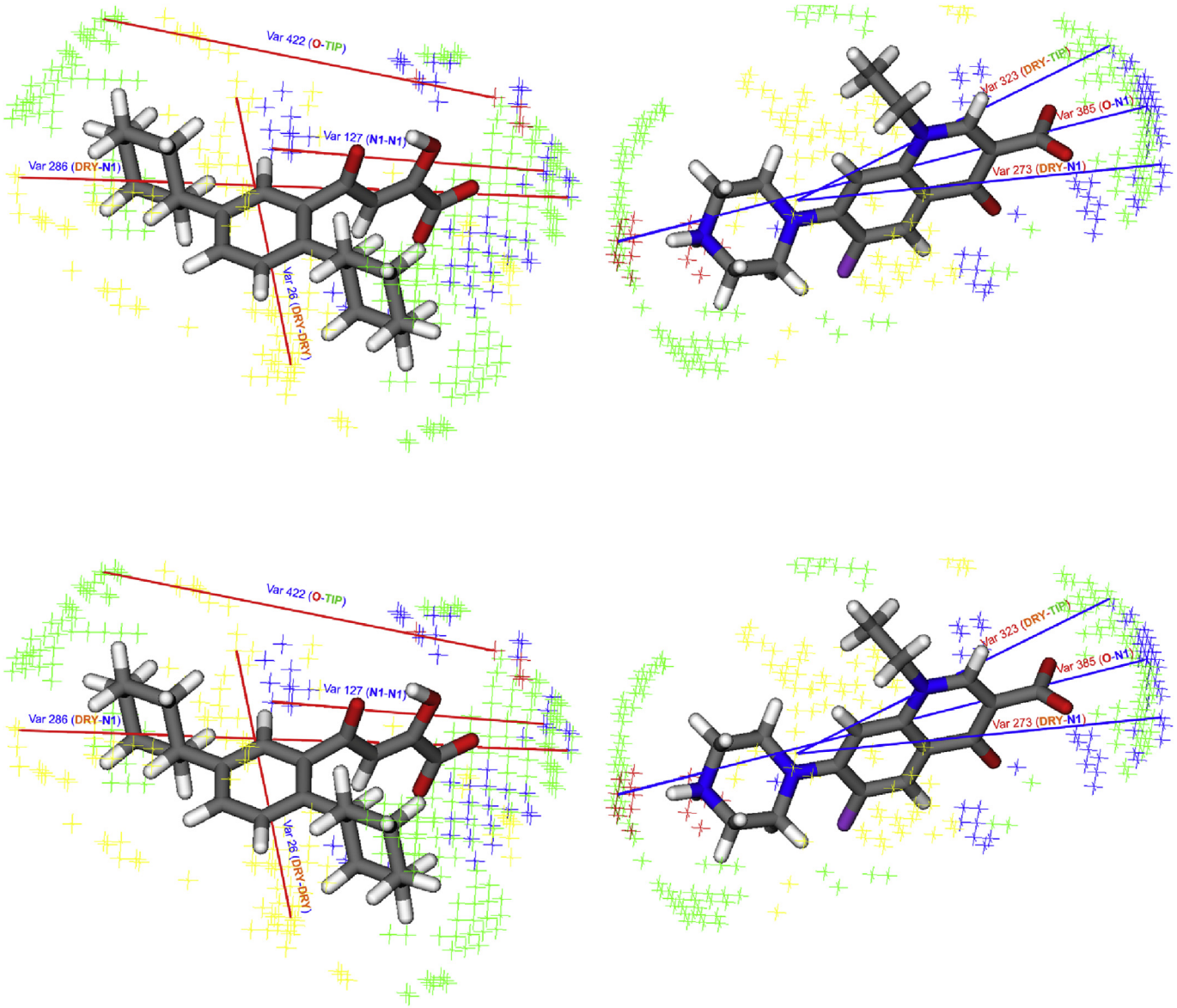

Fig. 8. Variables having highest impact on antibacterial activity of compounds represented using compound **12** as potent (red lines), and norfloxacin as less potent compound (blue lines). (For interpretation of the references to colour in this figure legend, the reader is referred to the web version of this article.)

3.5.2. Analysis of binding equilibria – binding constant and the number of binding sites

When small molecules bind independently to a set of equivalent sites on the protein, the equilibrium between free and bound molecules, for the static quenching process, is given by Equation (5):

$$\log\frac{F_0 - F}{F} = \log K_b + n\log[\mathrm{Q}] \tag{5}$$

where F_0 and F have the same meaning as in previous equations; K_b is the binding constant, and n is the number of binding sites. Linear dependence is shown in Fig. 13, and the results of linear regression analysis are given in Table 9.

Compound **12** binds to one independent binding site ($n \sim 1$, Table 9). As can be seen in Table 9, logK_b value decreases with the increase of temperature, which is an indication of static quenching mechanism.

3.5.3. Thermodynamic binding parameters

The enthalpy (ΔH) and entropy change (ΔS) during the binding of small molecule to protein can be determined measuring the binding constants at several temperatures, and following the Van't Hoff Equation (6):

$$\ln K = -\frac{\Delta H}{RT} + \frac{\Delta S}{R} \tag{6}$$

where R is the universal gas constant, T is the temperature (in K), and K is the S-V's binding constant at the corresponding temperature. Results are shown in Fig. 14 and Table 10.

According to Ross' view [45] the signs and magnitudes of thermodynamic parameters for protein reactions can account for the main forces contributing to protein stability. From the thermodynamic stand-point, $\Delta H>0$ and $\Delta S>0$ implies a hydrophobic interaction, $\Delta H<0$ and $\Delta S<0$ reflects the van der Waals force or hydrogen bond formation and $\Delta H<0$ and $\Delta S>0$ suggesting an electrostatic force.

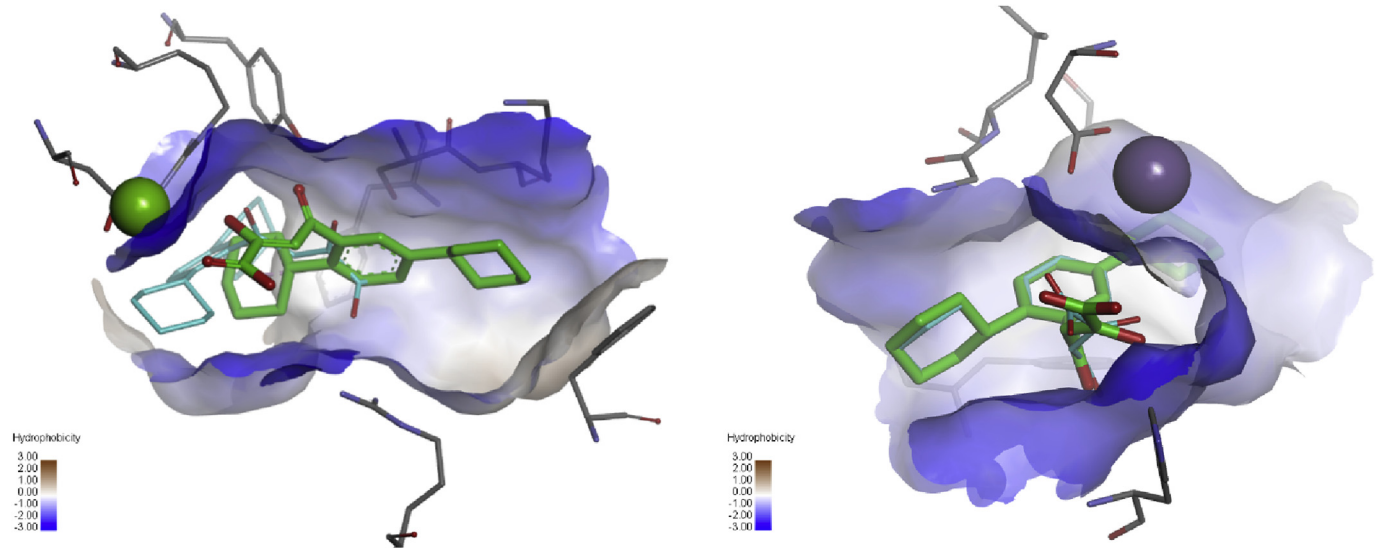

Fig. 9. The orientation of the most active compound **12** in *S. aureus* CrtM (left) and DNA Gyrase (right) binding sites. Active sites are represented as surfaces coloured according to hydrophobicity and protein residues that are 5 Å away from the ligand. The docked poses of monoanionic form (thick sticks with carbon atoms in green color) and dianionic form (thick sticks with carbon atoms in cyan color) are overlaid. Hydrogen atoms are not shown for clarity. (For interpretation of the references to colour in this figure legend, the reader is referred to the web version of this article.)

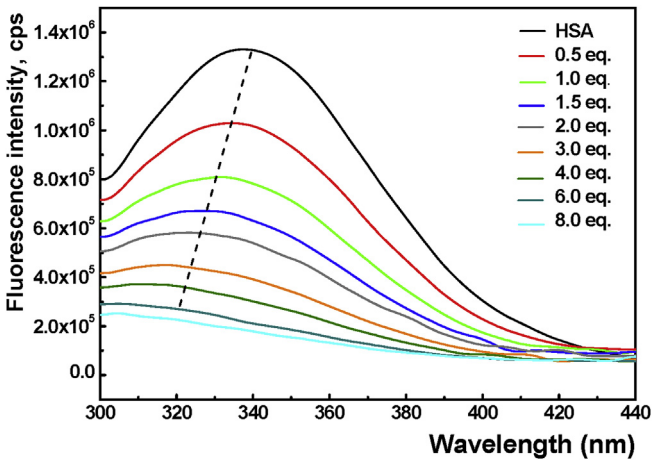

Fig. 10. Changes in HSA fluorescence emission spectra (c = 0.5 μM) upon addition of comp. **12** (c_{12} = 0.0; 0.25; 0.5; 0.75; 1; 1.5; 2.0; 3.0; 4.0 μM); T = 303 K; 30 mM PBS, pH = 7.38.

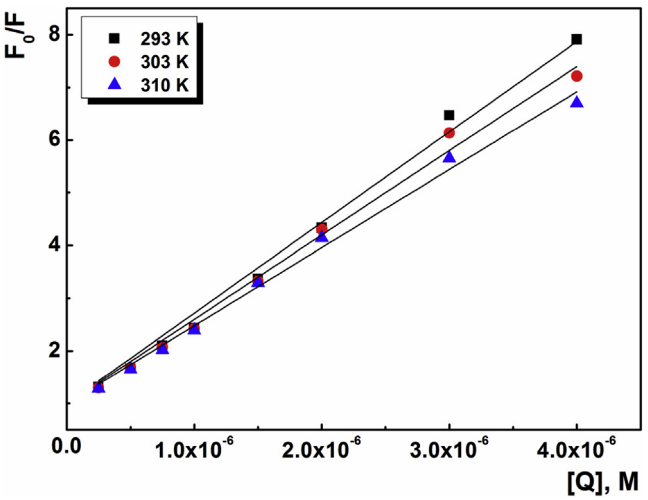

Fig. 11. S-V plot for binding of comp. **12** (0.5–8.0 eq.) to HSA (c = 0.5 μM) at three temperatures (293, 303 and 310 K); pH = 7.38 (30 mM PBS).

The negative enthalpy and positive entropy change indicate that the electrostatic forces are dominant for binding of **12** to HSA. Entropic term ($T\Delta S$) is the main contributor to overall free energy of binding.

We might draw the conclusion that compound **12** strongly binds to HSA and quenches its fluorescence intensity through static quenching mechanism. Trp214 as a main fluorophore of HSA is fully accessible for quenching with **12**. Although HSA possesses many binding sites, **12** binds to one independent binding site. Electrostatic forces are the principal forces responsible for the formation of **12**–HSA complex, with the entropic term being the main contributor to the free energy of binding.

The binding constant of **12** to HSA is relatively high, but still around one order of magnitude lower than the binding constant of myristic acid [46]. Therefore, this molecule can be efficiently stored and transported in the body. Potential problems with pharmacokinetics of this molecule may be overcome by making conjugates with HSA as a drug carrier, a strategy often employed in active therapeutics development [47].

Table 7
S-V constants at three temperatures; τ_0 = 7.09 ns. K_{sv} is obtained as a slope, while the intercept value was fixed as 1 (equation (3)).

T (K)	$K_{sv} \times 10^6$ (M^{-1})	$K_q \times 10^{14}$ (M^{-1} s^{-1})	r^2
293	1.72 ± 0.04	2.42	0.997
303	1.60 ± 0.03	2.26	0.998
310	1.48 ± 0.03	2.09	0.998

3.5.4. Acidity constants of 12

Aryldiketo acids in aqueous solution act as diprotic acids. pK_a Value of carboxylic group is near 2 (pK_{a1}), [48]; the second proton dissociates from enolic –OH group (pK_{a2} value around 7). Spectrophotometric titration was used to experimentally determine pK_a

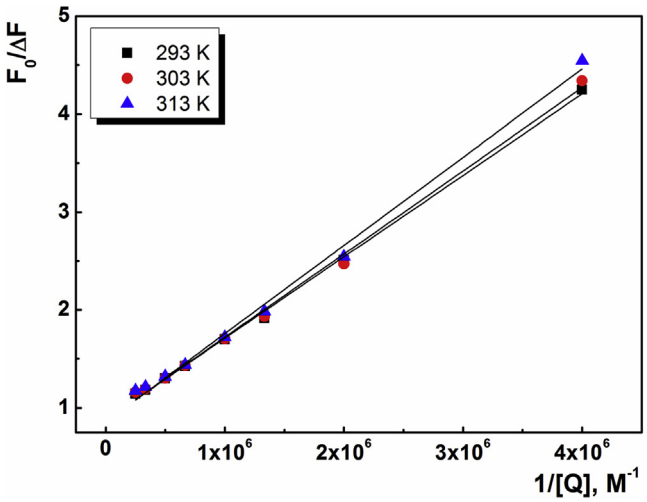

Fig. 12. Modified S-V plot for binding of **12** (0.5–8.0 eq.) to HSA (c = 0.5 μM) at three temperatures (293, 303 and 310 K); pH = 7.38 (30 mM PBS).

Table 8
Effective quenching constants at three temperatures.

T (K)	$K_a \times 10^6$ (M^{-1})	f_a	r^2
293	1.06 ± 0.02	1.14 ± 0.03	0.998
303	1.02 ± 0.03	1.15 ± 0.05	0.996
310	0.95 ± 0.03	1.17 ± 0.06	0.994

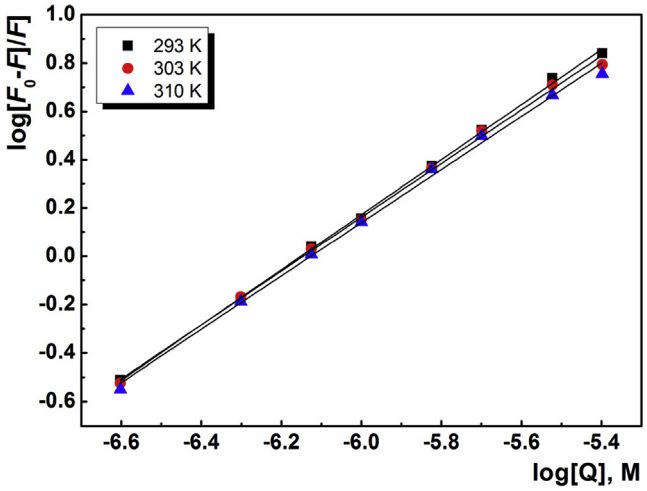

Fig. 13. Log-log plot for determination of binding constant (logK_b), and the number of binding sites (n) for binding of **12** to HSA at three temperatures.

Table 9
Binding constant (logK_b) and the number of binding sites (n) for binding of **12** to HSA at three temperatures.

T (K)	logK_b (M^{-1})	n	r^2
293	7.02 ± 0.09	1.14 ± 0.02	0.999
303	6.84 ± 0.12	1.11 ± 0.02	0.998
310	6.75 ± 0.15	1.10 ± 0.03	0.996

values of **12**. Absorption spectra changes of **12** with pH change are shown in Fig. 15. The existence of clearly visible isosbestic point at 278.3 nm proves that the dissociation of −OH group is the only

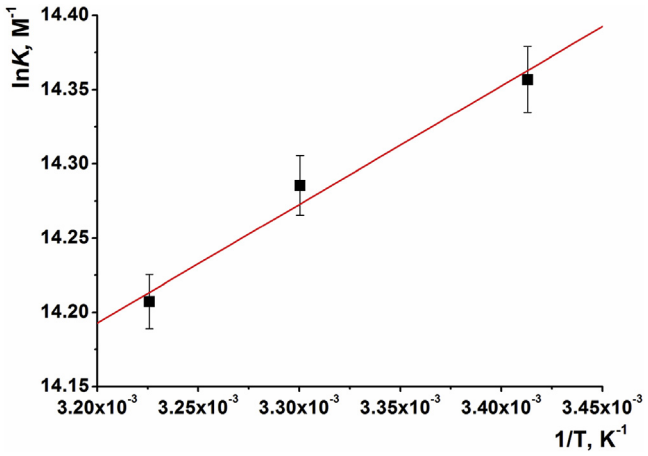

Fig. 14. The plot of ln$K$ *vs.* 1/T for the interaction of **12** with HSA.

Table 10
Thermodynamic parameters of compound's **12** binding to HSA.

T (K)	ln$K$ (M^{-1})	ΔG (kJmol^{-1})	ΔH (kJmol^{-1})	ΔS (Jmol^{-1}K^{-1})
293	14.36	34.97	−6.64	96.76
303	14.29	35.99		
310	14.21	36.62		

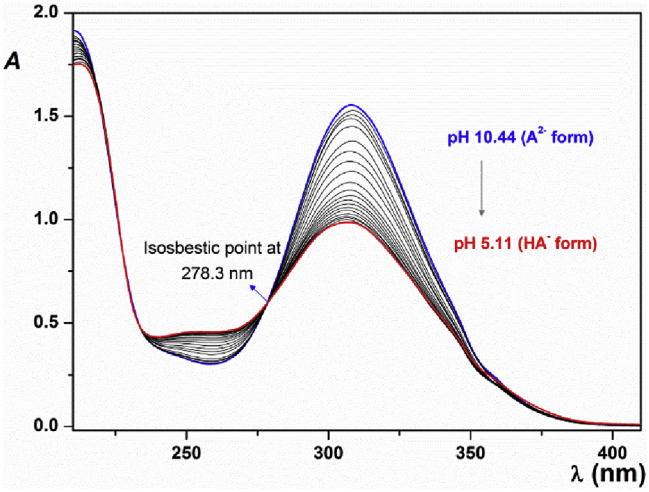

Fig. 15. Absorption spectra of **12** used for pK_{a2} value determination (fully deprotonated, A^{2-}, form is shown as blue line, HA^- form shown as red line). (For interpretation of the references to colour in this figure legend, the reader is referred to the web version of this article.)

process going on in the solution within studied pH range. Spectral data are processed according to equation (1) and pK_{a2} value 7.56 ± 0.04 is obtained. In solutions with pH < 4, where **12** is present in H_2A and/or HA^- form, solubility is lower, thus compound **12** precipitates. Therefore, the pK_{a1} value of **12** could not be determined under these experimental conditions. According to pK_{a2} value, pH-dependent distribution of HA^- and A^{2-} was calculated: at blood pH value (7.4), compound **12** exists as a mixture of monoanionic (59% HA^-) and dianionic form (41% A^{2-}).

3.5.5. log$D_{7.4}$ determination of compound 12

The log$D_{7.4}$ value (log$D$ = 2.6 ± 0.1) was determined using

shake-flask method.

4. Conclusions

The aim of this work was to design and synthesize a series of novel analogues of aryl diketo acids (ADKs) that have antimicrobial activity against multidrug resistant Gram positive bacterial strains. Among them, compound **12** having 2,5 di-cyclohexyl substitution at the aryl moiety, has exhibited a promising activity against a number of multidrug resistant strains and ten folds higher activity than the standard antibiotic norfloxacin. Through molecular docking approach and synthesis of active molecules analogues, we had demonstrated that diketo moiety is responsible for antimicrobial activity of this series, most likely through sequestering divalent ions in the active sites of several target proteins. This may provide a potential to simultaneously affect different biochemical pathways in bacteria and thus minimize the development of resistance against this class of molecules. Albeit the most active compound has high affinity for serum albumin, this class of molecules may serve as a good structural source for further lead optimization through conjugation to serum albumin or a development of novel antimicrobials through further rational modifications to allow targeting of relevant enzymes in Gram negative bacteria.

Conflict of interest

The authors confirm that this article content has no conflict of interest.

Acknowledgements

Ministry of Education, Science and Technological Development of the Republic of Serbia supported this work, Grant No. 172035. University of Hertfordshire is acknowledged for its support to the project.

Appendix A. Supplementary data

Supplementary data associated with this article can be found in the online version, at https://doi.org/10.1016/j.ejmech.2017.10.045. These data include MOL files and InChiKeys of the most important compounds described in this article.

References

[1] E. Oldfield, X. Feng, Resistance-resistant antibiotics, Trends Pharmacol. Sci. 35 (2014) 664–674, https://doi.org/10.1016/j.tips.2014.10.007.
[2] F. Rossi, L. Diaz, A. Wollam, D. Panesso, Y. Zhou, S. Rincon, A. Narechania, G. Xing, T.S.R. Di Gioia, A. Doi, T.T. Tran, J. Reyes, J.M. Munita, L.P. Carvajal, A. Hernandez-Roldan, D. Brandão, I.M. van der Heijden, B.E. Murray, P.J. Planet, G.M. Weinstock, C.A. Arias, Transferable vancomycin resistance in a community-associated MRSA lineage, N. Engl. J. Med. 370 (2014) 1524–1531, https://doi.org/10.1056/NEJMoa1303359.
[3] W. Zhu, Y. Zhang, W. Sinko, M.E. Hensler, J. Olson, K.J. Molohon, S. Lindert, R. Cao, K. Li, K. Wang, Y. Wang, Y.-L. Liu, A. Sankovsky, C.A.F. de Oliveira, D. a Mitchell, V. Nizet, J.A. McCammon, E. Oldfield, Antibacterial drug leads targeting isoprenoid biosynthesis, Proc. Natl. Acad. Sci. U. S. A. 110 (2013) 123–128, https://doi.org/10.1073/pnas.1219899110.
[4] G.Y. Liu, A. Essex, J.T. Buchanan, V. Datta, H.M. Hoffman, J.F. Bastian, J. Fierer, V. Nizet, Staphylococcus aureus golden pigment impairs neutrophil killing and promotes virulence through its antioxidant activity, J. Exp. Med. 202 (2005) 209–215, https://doi.org/10.1084/jem.20050846.
[5] C.-I. Liu, G.Y. Liu, Y. Song, F. Yin, M.E. Hensler, W.-Y. Jeng, V. Nizet, A.H.-J. Wang, E. Oldfield, A cholesterol biosynthesis inhibitor blocks Staphylococcus aureus virulence, Sci. 319 (2008) 1391–1394, https://doi.org/10.1126/science.1153018.
[6] B.J. Drakulić, M. Stavri, S. Gibbons, Ž.S. Žižak, T.Ž. Verbić, I.O. Juranić, M. Zloh, Aryldiketo acids have antibacterial activity against MDR Staphylococcus aureus strains: structural insights based on similarity and molecular interaction fields, ChemMedChem. 4 (2009) 1971–1975, https://doi.org/10.1002/cmdc.200900273.
[7] J.A. Grobler, K. Stillmock, B. Hu, M. Witmer, P. Felock, A.S. Espeseth, A. Wolfe, M. Egbertson, M. Bourgeois, J. Melamed, J.S. Wai, S. Young, J. Vacca, D.J. Hazuda, Diketo acid inhibitor mechanism and HIV-1 integrase: implications for metal binding in the active site of phosphotransferase enzymes, Proc. Natl. Acad. Sci. 99 (2002) 6661–6666, https://doi.org/10.1073/pnas.092056199.
[8] Y. Zhang, Fu-Yang Lin, K. Li, W. Zhu, Y. Liu, R. Cao, R. Pang, E. Lee, J. Axelson, M. Hensler, K. Wang, K.J. Molohon, Y. Wang, D.A. Mitchell, V. Nizet, E. Oldfield, HIV-1 integrase inhibitor-inspired antibacterials targeting isoprenoid biosynthesis, ACS Med. Chem. Lett. 3 (2012) 402–406, https://doi.org/10.1021/ml300038t.
[9] O.A. Sof'ina, N.M. Igidov, E.N. Koz'minykh, N.N. Trapeznikova, Y.S. Kasatkina, V.O. Koz'minykh, Reactions of acylpyruvic acids and 2,3-dihydrofuran-2,3-diones with 2,3-diaminopyridine, Russ. J. Org. Chem. 37 (2001) 1017–1025, https://doi.org/10.1023/A:1012438902959.
[10] I.N. Cvijetić, T.Ž. Verbić, B.J. Drakulić, D.M. Stanković, I.O. Juranić, D.D. Manojlović, M. Zloh, Redox properties of alkyl-substituted 4-aryl-2,4-dioxobutanoic acids, J. Serb. Chem. Soc. (2017), https://doi.org/10.2298/JSC161118021C.
[11] S. Gibbons, E.E. Udo, The effect of reserpine, a modulator of multidrug efflux pumps, on the in vitro activity of tetracycline against clinical isolates of methicillin resistant Staphylococcus aureus (MRSA) possessing the tet(K) determinant, Phyther. Res. 14 (2000) 139–140, https://doi.org/10.1002/(SICI)1099-1573(200003)14:2<139::AID-PTR608>3.0.CO;2–8.
[12] J.I. Ross, A.M. Farrell, E.A. Eady, J.H. Cove, W.J. Cunliffe, Characterisation and molecular cloning of the novel macrolide-streptogramin B resistance determinant from Staphylococcus epidermidis, J. Antimicrob. Chemother. 24 (1989) 851–862, https://doi.org/10.1093/jac/24.6.851.
[13] J.F. Richardson, S. Reith, Characterization of a strain of methicillin-resistant Staphylococcus aureus (EMRSA-15) by conventional and molecular methods, J. Hosp. Infect. 25 (1993) 45–52, https://doi.org/10.1016/0195-6701(93)90007-M.
[14] G.W. Kaatz, S.M. Seo, C.A. Ruble, Efflux-mediated fluoroquinolone resistance in Staphylococcus aureus, Antimicrob. Agents Chemother. 37 (1993) 1086–1094.
[15] E.C. for A.S.T. (EUCAST) of the E.S. of C.M. and I.D. (ESCMID), Determination of minimum inhibitory concentrations (MICs) of antibacterial agents by broth dilution, Clin. Microbiol. Infect. 9 (2003) ix–xv, https://doi.org/10.1046/j.1469-0691.2003.00790.x.
[16] T.S. Rush, J.A. Grant, L. Mosyak, A. Nicholls, A shape-based 3-D Scaffold Hopping method and its application to a bacterial Protein–Protein interaction, J. Med. Chem. 48 (2005) 1489–1495, https://doi.org/10.1021/jm040163o.
[17] D. Bajusz, A. Rácz, K. Héberger, Why is Tanimoto index an appropriate choice for fingerprint-based similarity calculations? J. Cheminform 7 (2015) 1–13, https://doi.org/10.1186/s13321-015-0069-3.
[18] P.C.D. Hawkins, A.G. Skillman, G.L. Warren, B.A. Ellingson, M.T. Stahl, Conformer generation with OMEGA: algorithm and validation using high quality structures from the protein databank and Cambridge structural database, J. Chem. Inf. Model 50 (2010) 572–584, https://doi.org/10.1021/ci100031x.
[19] T.A. Halgren, MMFF VI. MMFF94s option for energy minimization studies, J. Comput. Chem. 20 (1999) 720–729, https://doi.org/10.1002/(SICI)1096-987X(199905)20:7<720::AID-JCC7>3.0.CO;2-X.
[20] J.J.P. Stewart, Optimization of parameters for semiempirical methods V: modification of NDDO approximations and application to 70 elements, J. Mol. Model 13 (2007) 1173–1213, https://doi.org/10.1007/s00894-007-0233-4.
[21] J.J.P. Stewart, MOPAC: a semiempirical molecular orbital program, J. Comput. Aided. Mol. Des. 4 (1990) 1–105, https://doi.org/10.1007/BF00128336.
[22] P.J. Goodford, A computational procedure for determining energetically favorable binding sites on biologically important macromolecules, J. Med. Chem. 28 (1985) 849–857, https://doi.org/10.1021/jm00145a002.
[23] F. Fontaine, M. Pastor, F. Sanz, Incorporating molecular shape into the alignment-free GRid-INdependent descriptors, J. Med. Chem. 47 (2004) 2805–2815, https://doi.org/10.1021/jm0311240.
[24] M. Clark, R.D. Cramer, The probability of chance correlation using partial least squares (PLS), Quant. Struct. Relat. 12 (1993) 137–145, https://doi.org/10.1002/qsar.19930120205.
[25] G. Klebe, U. Abraham, T. Mietzner, Molecular similarity indices in a comparative analysis (CoMSIA) of drug molecules to correlate and predict their biological activity, J. Med. Chem. 37 (1994) 4130–4146, https://doi.org/10.1021/jm00050a010.
[26] A.A. Alizadeh, M. Hamzeh-Mivehroud, B. Sokouti, S. Dastmalchi, An alignment-independent 3D-QSAR study on series of hydroxamic acid-based tumor necrosis factor-α converting enzyme inhibitors, J. Chemom. (2016) 537–547, https://doi.org/10.1002/cem.2817.
[27] I.N. Cvijetić, Ž.P. Žižak, T.P. Stanojković, Z.D. Juranić, N. Terzić, I.M. Opsenica, D.M. Opsenica, I.O. Juranić, B.J. Drakulić, An alignment independent 3D QSAR study of the antiproliferative activity of 1,2,4,5-tetraoxanes, Eur. J. Med. Chem. 45 (2010) 4570–4577, https://doi.org/10.1016/j.ejmech.2010.07.019.
[28] L.M. Kabeya, C.H.T.P. da Silva, A. Kanashiro, J.M. Campos, A.E.C.S. Azzolini, A.C.M. Polizello, M.T. Pupo, Y.M. Lucisano-Valim, Inhibition of immune complex-mediated neutrophil oxidative metabolism: a pharmacophore model for 3-phenylcoumarin derivatives using GRIND-based 3D-QSAR and 2D-QSAR procedures, Eur. J. Med. Chem. 43 (2008) 996–1007, https://doi.org/

10.1016/j.ejmech.2007.07.003.
[29] I. Jabeen, P. Wetwitayaklung, P. Chiba, M. Pastor, G.F. Ecker, 2D- and 3D-QSAR studies of a series of benzopyranes and benzopyrano[3,4b][1,4]-oxazines as inhibitors of the multidrug transporter P-glycoprotein, J. Comput. Aided. Mol. Des. 27 (2013) 161–171, https://doi.org/10.1007/s10822-013-9635-9.
[30] Á. Durán, G.C. Martínez, M. Pastor, Development and validation of AMANDA, a new algorithm for selecting highly relevant regions in molecular interaction fields, J. Chem. Inf. Model 48 (2008) 1813–1823, https://doi.org/10.1021/ci800037t.
[31] M. Baroni, G. Costantino, G. Cruciani, D. Riganelli, R. Valigi, S. Clementi, Generating optimal linear PLS estimations (GOLPE): an advanced chemometric tool for handling 3D-QSAR problems, Quant. Struct. Relat. 12 (1993) 9–20, https://doi.org/10.1002/qsar.19930120103.
[32] X. Liu, S. Ouyang, B. Yu, Y. Liu, K. Huang, J. Gong, S. Zheng, Z. Li, H. Li, H. Jiang, PharmMapper server: a web server for potential drug target identification using pharmacophore mapping approach, Nucleic Acids Res. 38 (2010) W609–W614, https://doi.org/10.1093/nar/gkq300.
[33] B. Ojha, G. Das, The interaction of 5-(Alkoxy)naphthalen-1-amine with bovine serum albumin and its effect on the conformation of protein, J. Phys. Chem. B 114 (2010) 3979–3986, https://doi.org/10.1021/jp907576r.
[34] E.P. Serjeant, A. Albert, The Determination of Ionization Constants: a Laboratory Manual, second ed., Chapman and Hall, London, 1971.
[35] U. EPA, Product Properties Test Guidelines OPPTS 830.7550 Partition Coefficient (n-Octanol/Water), Shake Flask Method, Washington, 1996.
[36] A. Andres, M. Roses, C. Rafols, E. Bosch, S. Espinosa, V. Segarra, J.M. Huerta, Setup and validation of shake-flask procedures for the determination of partition coefficients (log D) from low drug amounts, Eur. J. Pharm. Sci. 76 (2015) 181–191, https://doi.org/10.1016/j.ejps.2015.05.008.
[37] EUCAST, Determination of minimum inhibitory concentrations (MICs) of antibacterial agents by broth dilution, Clin. Microbiol. Infect. 9 (2003) ix–xv, https://doi.org/10.1046/j.1469-0691.2003.00790.x.
[38] S. Gibbons, M. Oluwatuyi, G.W. Kaatz, A novel inhibitor of multidrug efflux pumps in Staphylococcus aureus, J. Antimicrob. Chemother. 51 (2003) 13–17, https://doi.org/10.1093/jac/dkg044.
[39] T.Ž. Verbić, B.J. Drakulić, M. Zloh, I.O. Juranić, The effect of phenyl substituents on C-13 NMR shifts and metal ions binding to 4-phenyl-2,4-dioxobutanoic acid derivatives, Lett. Org. Chem. 5 (2008) 692–699, https://doi.org/10.2174/157017808786857589.
[40] N.M. Vandevelde, P.M. Tulkens, F. Van Bambeke, Modulating antibiotic activity towards respiratory bacterial pathogens by co-medications: a multi-target approach, Drug Discov. Today 21 (2016) 1114–1129, https://doi.org/10.1016/j.drudis.2016.04.001.
[41] X.M. He, D.C. Carter, Atomic structure and chemistry of human serum albumin, Nature 358 (1992) 209–215.
[42] J.R. Lakowicz, Principles of Fluorescence Spectroscopy, third ed., Springer, US, 2006 https://doi.org/10.1007/978-0-387-46312-4.
[43] M. Amiri, K. Jankeje, J.R. Albani, Origin of fluorescence lifetimes in human serum albumin. Studies on native and denatured protein, J. Fluoresc. 20 (2010) 651–656, https://doi.org/10.1007/s10895-010-0597-1.
[44] M.R. Eftink, C.A. Ghiron, Fluorescence quenching studies with proteins, Anal. Biochem. 114 (1981) 199–227, https://doi.org/10.1016/0003-2697(81)90474-7.
[45] P.D. Ross, S. Subramanian, Thermodynamics of protein association reactions: forces contributing to stability, Biochemistry 20 (1981) 3096–3102, https://doi.org/10.1021/bi00514a017.
[46] A.O. Pedersen, R. Brodersen, Myristic acid binding to human serum albumin investigated by dialytic exchange rate, J. Biol. Chem. 263 (1988) 10236–10239.
[47] B. Elsadek, F. Kratz, Impact of albumin on drug delivery — new applications on the horizon, J. Control. Release 157 (2012) 4–28, https://doi.org/10.1016/j.jconrel.2011.09.069.
[48] T.Ž. Verbić, B.J. Drakulić, M.F. Zloh, J.R. Pecelj, G.V. Popović, I.O. Juranić, An LFER study of the protolytic equilibria of 4-aryl-2,4-dioxobutanoic acids in aqueous solutions, J. Serb. Chem. Soc. 72 (2007) 1201–1216, https://doi.org/10.2298/JSC0712201V.